iScience

CellPress

Article

Using Gene Editing to Establish a Safeguard System for Pluripotent Stem-Cell-Based Therapies

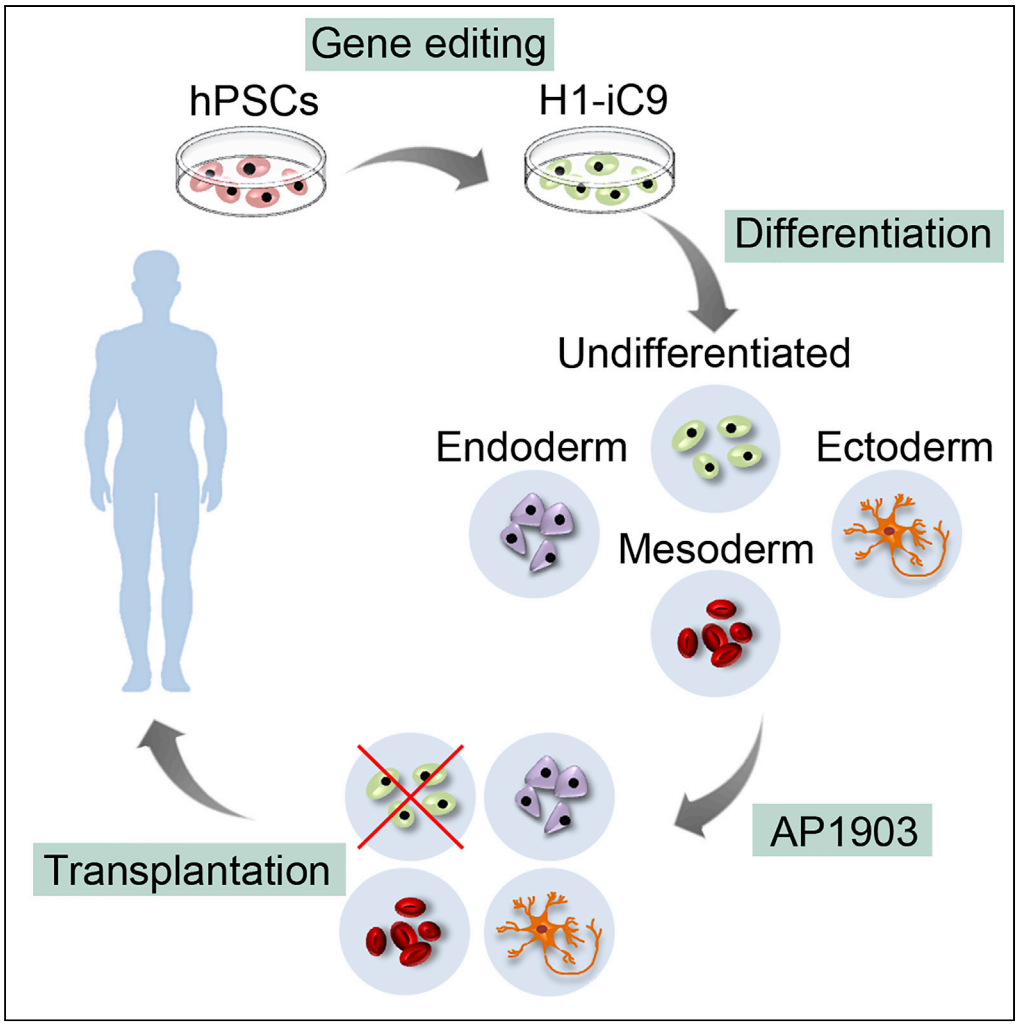

Youjun Wu, Tammy Chang, Yan Long, He Huang, Fouad Kandeel, Jiing-Kuan Yee

jyee@coh.org

HIGHLIGHTS

In-frame *iC9* gene insertion into the *SOX2* locus to target undifferentiated hESCs

The residual ESCs are selectively removed without affecting their differentiated progeny

Eradication of residual ESCs before transplantation provides an extra safety control

Wu et al., iScience *22*, 409–422 December 20, 2019
https://doi.org/10.1016/j.isci.2019.11.038

iScience

CellPress

Article

Using Gene Editing to Establish a Safeguard System for Pluripotent Stem-Cell-Based Therapies

Youjun Wu,[1] Tammy Chang,[1] Yan Long,[1,2] He Huang,[2] Fouad Kandeel,[1] and Jiing-Kuan Yee[1,3,*]

SUMMARY

A major challenge in using human pluripotent stem cells (hPSCs) in therapy is the risk of teratoma formation due to contaminating undifferentiated stem cells. We used CRISPR-Cas9 for in-frame insertion of a suicide gene, *iC9*, into the endogenous *SOX2* locus in human embryonic stem cell (ESC) line H1 for specific eradication of undifferentiated cells without affecting differentiated cells. This locus was chosen over *NANOG* and *OCT4*, two other well-characterized stem cell loci, due to significantly reduced off-target effect. We showed that undifferentiated H1-iC9 cells were induced to apoptosis by iC9 inducer AP1903, whereas differentiated cell lineages including hematopoietic cells, neurons, and islet beta-like cells were not affected. We also showed that AP1903 selectively removed undifferentiated H1-iC9 cells from a mixed cell population. This strategy therefore provides a layer of safety control before transplantation of a stem-cell-derived product in therapy.

INTRODUCTION

One of the many promises of hPSCs is to provide a platform to support the treatment of human diseases (Thomson et al., 1998). Protocols built on knowledge gained from studying the developmental cues for a particular tissue or organ have been established to guide hPSC differentiation (Klimanskaya et al., 2004; Ng et al., 2005; Pagliuca et al., 2014; Rezania et al., 2014; Talkhabi et al., 2016; Wichterle et al., 2002). Although most hPSC-derived cells are not functionally mature as their counterparts in adult tissues, a few of them including cardiomyocytes, retina pigment epithelial cells, and pancreatic progenitor cells have entered clinical trials or are set to enter clinical trials soon (Menasche et al., 2018; Schwartz et al., 2015; Song et al., 2015). Despite these progresses, important challenges remain. One major challenge is the risk of teratoma formation due to contamination of undifferentiated hPSCs in hPSC-derived cell products. In almost all cases, stem-cell-derived cell products are comprised of a mixed cell population with the desired cell type constituting only a fraction of the entire population. If sufficient quantities of undifferentiated hPSCs remained, they could form teratomas in patients upon transplantation (Hentze et al., 2009). This risk represents a major hurdle in using hPSCs in cell-based therapy.

The use of a suicide gene to selectively eradicate undifferentiated hPSCs represents an appealing strategy to address this hurdle (Li and Xiang, 2013). It relies on the ability of the suicide gene product to convert a non-toxic and bio-inert prodrug into a cytotoxic product that triggers cell death. Selective expression of a suicide gene only in undifferentiated hPSCs would remove these cells from differentiated cell products. Previous attempts to express suicide genes to control graft-versus-host disease or to ablate transformed cells mainly relied on random insertion of the suicide gene into host chromosomes (Bonini et al., 1997; Zarogoulidis et al., 2013). Limiting suicide gene expression only in undifferentiated hPSCs with such a strategy would be difficult. Random gene insertion also increases the risk of insertional mutagenesis (Bokhoven et al., 2009). Modulating expression of a suicide gene from stem cell loci addresses these concerns. Direct control of the suicide gene from a stem cell locus ensures rapid shutdown of the suicide gene once hPSCs are committed to differentiate. Precise gene insertion also avoids the risk of insertional mutagenesis.

In-frame insertion of a fluorescence reporter into the well-characterized stem cell *OCT4* locus in hPSCs for monitoring cell-fate decision in real time has been reported previously (Balboa et al., 2017; Hockemeyer et al., 2009; Krentz et al., 2014; Zhu et al., 2015). However, close examination of the sequence near the *OCT4* stop codon, the target site for in-frame gene insertion, revealed multiple genomic sites with similar or identical sequences (Figure S1). It is likely that these off-target sites would be cleaved by the *OCT4*-specific nucleases used in those studies and generate insertion-deletion (indel) or other lesions such as

[1]Departments of Translational Research & Cellular Therapeutics, Beckman Research Institute of City of Hope, Duarte, CA 91010, USA

[2]Bone Marrow Transplantation Center, The First Affiliated Hospital, Zhejiang University, Hangzhou, Zhejiang 310027, China

[3]Lead Contact

*Correspondence: jyee@coh.org

https://doi.org/10.1016/j.isci.2019.11.038

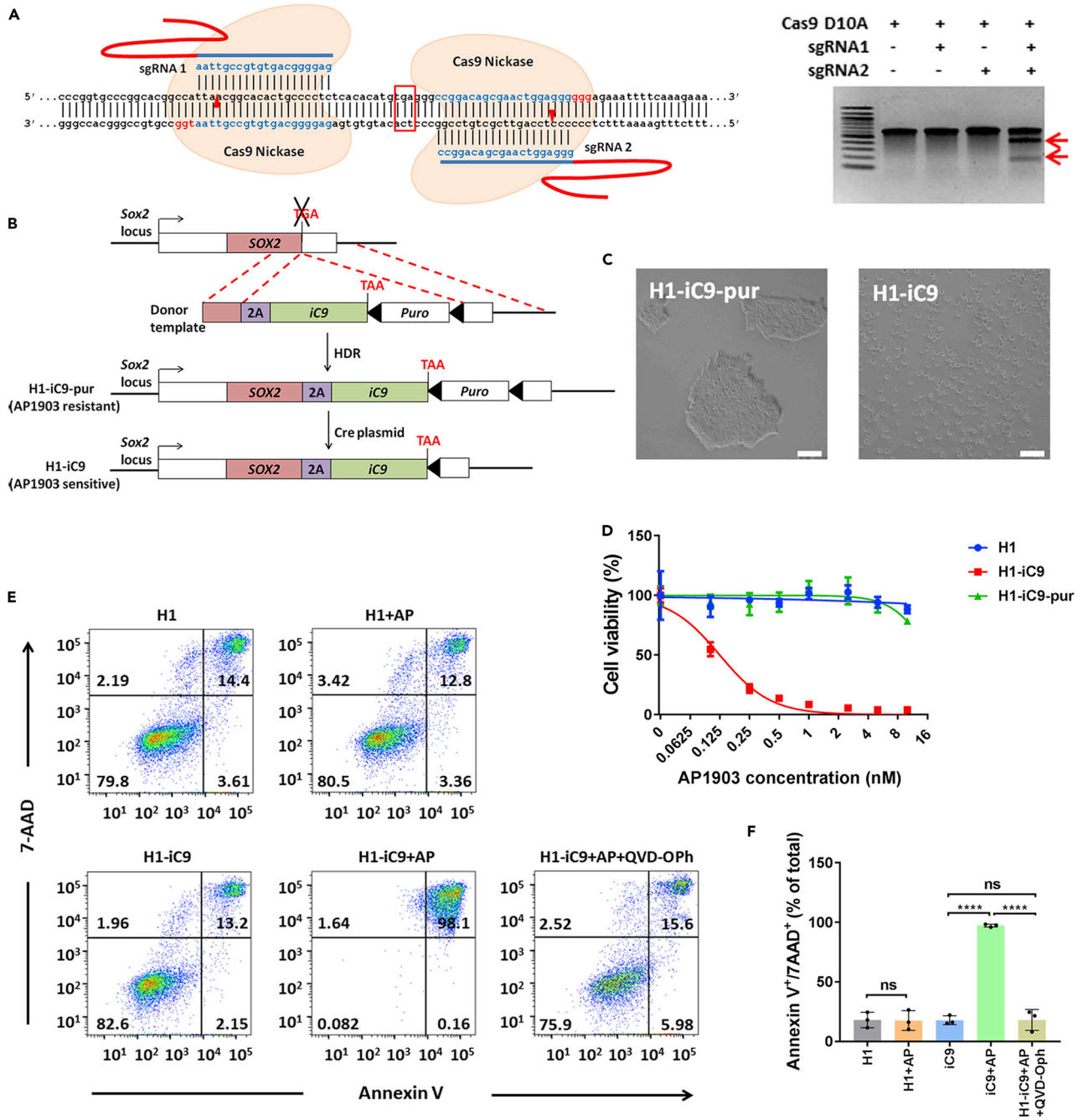

Figure 1. CRISPR-Cas9-Mediated *iC9* Gene Insertion into the *SOX2* Locus Renders H1 Cells Susceptible to the Killing by AP1903

(A) Left: sequences of sgRNA1, sgRNA2, and their genomic targets in the *SOX2* locus. Stop codon of the *SOX2* coding region is boxed. PAM sequence is labeled in red. Cleavage site of CRISPR-Cas9 is marked by the red arrowhead. Right: Cas9 D10A nickase-mediated cleavage of the *SOX2* genomic target was analyzed by the Surveyor assay in transiently transfected HEK293T cells. Two red arrows mark the expected cleavage products.

(B) Scheme to use CRISPR-Cas9 to establish H1 clones with in-frame insertion of the *2A-iC9* transgene into the endogenous *SOX2* locus (H1-iC9-pur clone) and to remove the *Puro* gene by Cre/loxP-mediated excision (H1-iC9 clone). Broken lines specify the regions of homology between the donor template and the *SOX2* locus for homologous recombination. Filled arrowheads indicate the *loxP* site. HDR: homology-directed recombination.

(C) AP1903 treatment of H1-iC9-pur and H1-iC9 cells. Treatment was carried out overnight in media containing 100 nM AP1903. Scale bar = 50 μm.

(D) Cell viability after overnight treatment with AP1903 at the indicated concentration determined by MTS assay for H1, H1-iC9-pur, and H1-iC9 cells. The iC50 of AP 1903 in H1-iC9 cells was 0.1242 ± 0.0083 nM calculated from the dose-response curve. Values represent mean ± s.d. (*N* = 4 independent experiments).

Figure 1. *Continued*

(E and F) Analysis of apoptotic cells after overnight treatment with AP1903 at a concentration of 10 nM. qVD-Oph at a concentration of 20 mM was applied simultaneously with AP1903 for overnight treatment. Representative FACS profiles (E) and the bar graph that depicts Annexin V^+/$7AAD^+$ apoptotic cells from three independent experiments (F) were shown. Bars indicate the mean (±s.d.) of individual data points. ****$p < 0.0001$, ns: not statistically significant.

chromosome translocation, although such a possibility was not investigated in those studies. Because of the potential off-target effect with the nucleases used in the *OCT4* locus, we considered two other well-characterized stem cell loci, *NANOG* and *SOX2,* for suicide gene insertion. As the *OCT4* locus, several genomic sites exhibit sequence homology with the target site in the *NANOG* locus for in-frame gene insertion (Figure S1). In contrast, only one additional genomic site exhibits such sequence homology with the target site in the *SOX2* locus (Figure S1). To minimize the off-target effect, we therefore focused our effort in the current study on the insertion of a suicide gene into the *SOX2* locus for selective eradication of undifferentiated hPSCs.

Two suicide strategies are widely used in cell-based therapy, including herpes simplex virus thymidine kinase (HSV-TK) and inducible caspsae-9 (iC9) (Zarogoulidis et al., 2013). HSV-TK induces cell death by converting the non-toxic prodrug ganciclovir (GCV) into a toxic form to block DNA replication (Moolten, 1986; Reardon, 1989). Multiple studies have demonstrated the effectiveness of expressing HSV-TK to kill undifferentiated hPSCs (Liang et al., 2018; Schuldiner et al., 2003). Since this system relies on cell division, it is not suitable for treating proliferating cells such as differentiated progenitor cells to remove undifferentiated hPSCs. In the current study, we focused on the iC9 suicide system for the removal of contaminating undifferentiated hPSCs from stem cell-derived products before transplantation. The *iC9* suicide gene encodes a fusion protein between human Caspase 9 and FK506-binding protein (Straathof et al., 2005). Individual iC9 subunits do not induce cell apoptosis. Dimerization of the iC9 subunits can be induced by a small molecule AP1903, which is well tolerated in culture cells and in clinical studies (Clackson et al., 1998). Dimerization of iC9 activates one of the last steps in the apoptotic cascade, resulting in rapid cell death. To maintain stem cell pluripotency, levels of SOX2 need to be stringently regulated (Boer et al., 2007; Kopp et al., 2008). In-frame insertion of the *iC9* gene following the coding region of the *SOX2* gene minimizes the risk of disrupting normal SOX2 expression. In the current study, this site-specific gene insertion was achieved by using CRISPR-Cas9 in human embryonic stem cell (ESC) line H1. We showed that *iC9* gene insertion led to the eradication of undifferentiated H1 cells without affecting the viability of multiple H1-derived cell lineages, including hematopoietic cells, neurons, and pancreatic beta-like cells. Our results demonstrate that suicide gene insertion into the *SOX2* locus is an effective strategy to selectively eradicate undifferentiated hPSCs and prevent teratoma formation. This strategy therefore provides a layer of safety control to reduce the risk of using hPSC-derived cell products in therapy.

RESULTS

Stem Cells Expressing iC9 Are Selectively Eradicated by AP1903 Treatment

To selectively express iC9 in undifferentiated hPSCs but not in their differentiated progeny, we used CRISPR-Cas9 to insert the *iC9* gene into the *SOX2* locus in H1 cells. A pair of sgRNA targeting a region near the stop codon of the *SOX2* locus was designed (Figure 1A, left). This pair, sgRNA1 and sgRNA2, efficiently cleaved their target at the *SOX2* locus when co-expressed with Cas9 nickase (Ran et al., 2013), whereas Cas9 nickase with single sgRNA could not generate the cleavage (Figure 1A, right). Because a steady level of SOX2 is crucial for the maintenance of stem cell pluripotency and self-renewal, our strategy involves in-frame fusion of a *2A-iC9* transgene cassette into the *SOX2* locus to minimize the risk of disrupting *SOX2* expression (Figure 1B). Inclusion of the self-cleaving 2A peptide between the SOX2 and iC9 proteins is expected to facilitate normal production of SOX2. We used a donor template harboring the *2A-iC9* and the *puromycin-resistant* (*Puro*) gene encoding puromycin N-acetyl transferase flanked by homology arms spanning the stop codon of the *SOX2* gene for homologous recombination (Figures 1B and S2A). After puromycin selection, we picked three H1-iC9-pur clones containing monoallelic insertion of the *iC9* gene for further analysis (Figures S2B and S2C).

Treatment of H1-iC9-pur cells with 100 nM AP1903 led to no observable cell death (Figure 1C). Because previous studies showed that positive selection cassettes could interfere with the expression of the neighboring gene (Davis et al., 2008; Zhu et al., 2015), we delivered Cre-expressing plasmid into H1-iC9-pur clones by nucleofection to remove the *Puro* gene flanked by *loxP* sites and established

the H1-iC9 clones (Figures 1B and S3). Unlike H1-iC9-pur cells, AP1903 treatment efficiently eradicated H1-iC9 cells (Figure 1C). Karyotype analysis showed that both H1-iC9-pur and H1-iC9 are normal as parental H1 cells (Figure S4). To assay for off-target effect of the two sgRNAs used, we sequenced the potential off-target site on chromosome 8 (Figure S1) in H1-iC9 cells for indel formation and found none (data not shown). In addition, sequence analysis of the predicted top five off-target sites for each individual sgRNA exhibited no nucleotide changes (Table S1). These results are consistent with the previous report that the use of paired nickases in gene editing significantly reduced the off-target effect (Ran et al., 2013).

To assess the drug sensitivity, H1, H1-iC9-pur, and H1-iC9 cells were exposed to increasing concentrations of AP1903. A dose-dependent cytotoxicity of the drug was observed in H1-iC9 cells with an IC50 of 0.1242 nM, whereas the viability of parental H1 cells and H1-iC9-pur cells was not affected by the treatment (Figure 1D). AP1903-induced toxicity was further analyzed by flow cytometry (Figures 1E and 1F). There was no significant increase in apoptotic cells when H1 cells were exposed to 10 nM AP1903 relative to the untreated control. In contrast, the majority of H1-iC9 cells became apoptotic with the same treatment. Cell killing was mediated through the Caspase signaling pathway as demonstrated by the block of cell death with pan-Caspase inhibitor qVD-Oph (Figures 1E and 1F) (Caserta et al., 2003).

To determine whether AP1903 can selectively eradicate iC9-expressing cells, we transduced H1-iC9 cells with a GFP lentivirus (Figures S5A and 2A). The sorted GFP^+ cells, H1-iC9(GFP), were mixed with H1 cells. AP1903 exposure completely eradicated the population of H1-iC9(GFP) cells (Figures 2B–2D). Killing of the GFP^+ cell population was also detected by fluorescence microscopy, whereas most of the GFP^- cell remained viable with the drug treatment (Figure S5B). Inoculation of H1-iC9(GFP) cells into NOD *scid gamma* (NSG) mice led to the formation of teratomas containing cells derived from the three germ layers (Figure S6), suggesting that iC9 expression did not affect the pluripotency of H1 cells. To validate selective eradication of H1-iC9(GFP) cells from a mixed cell population, H1 and H1-iC9(GFP) cells mixed at a ratio of 1:1 were either mock treated or treated with AP1903 followed by transplantation into NSG mice (Figure 2E). Both GFP^+ and GFP^- cells were present in teratomas derived from mock treatment (Figure 2F). Treatment with AP1903 before transplantation gave rise to teratomas containing no detectable GFP^+ cells (Figure 2F). Taken together, these results demonstrated the susceptibility of iC9-expressing H1 cells to AP1903.

Resistance of H1-iC9-Derived Hematopoietic Cells to AP1903 Treatment

To determine the effect of iC9 on hPSC-derived cell lineages, we first differentiated H1-iC9 cells into hematopoietic cells (Figure 3A). AP1903 treatment of the hematopoietic populations derived from H1 and H1-iC9 cells showed little change in the percentage of apoptotic cells compared with mock control (Figures 3B and 3C). Flow cytometry analysis showed that the percentage of $CD45^+$ hematopoietic cells derived from H1 and H1-iC9 cells was not altered significantly by AP1903 treatment (Figures 3D and 3E). Quantitative RT-PCR analysis showed that *SOX2* transcript disappeared upon hematopoietic differentiation (Figure 3F). Thus, differentiation of H1-iC9 cells into the $CD45^+$ hematopoietic cell lineage silenced iC9 expression, rendering these cells resistant to AP1903-induced apoptosis.

Resistance of H1-iC9-Derived Neurons to AP1903 Treatment

SOX2 is known to express in neural progenitor cells (NPCs) where it regulates proliferation/survival and neurogenesis (Graham et al., 2003). However, its expression is down-regulated during terminal neuronal differentiation (Graham et al., 2003). We differentiated H1 and H1-iC9 cells into neurons (Figure 4A). Many cells in the differentiated culture expressed the terminal differentiated neuronal marker class III beta-tubulin (TuJ1) (Figure 4B). Although a portion of $SOX2^+$ cells existed in the differentiated neuronal culture derived from H1 and H1-iC9, the majority of $TuJ1^+$ neurons lacked SOX2 expression (Figure 4B). These $SOX2^+$ cells in the H1-iC9-derived culture were eradicated by AP1903 treatment, whereas most of the $TuJ1^+$ cells were not affected (Figure 4B). By contrast, AP1903 treatment did not seem to affect the viability of the $SOX2^+$ cells in the H1-derived culture. Immunofluorescence study confirmed that the $SOX2^+$ cells in the H1-iC9-derived culture were NPCs, which co-expressed the progenitor marker Nestin (Figure 4C). In support of this conclusion, we differentiated H1 and H1-iC9 cells into NPCs, and immunofluorescence staining demonstrated that the majority of the cells stained positive for both Nestin and SOX2 (Figure 4D). Quantitative real-time PCR showed that expression of *NANOG* and *OCT4* was

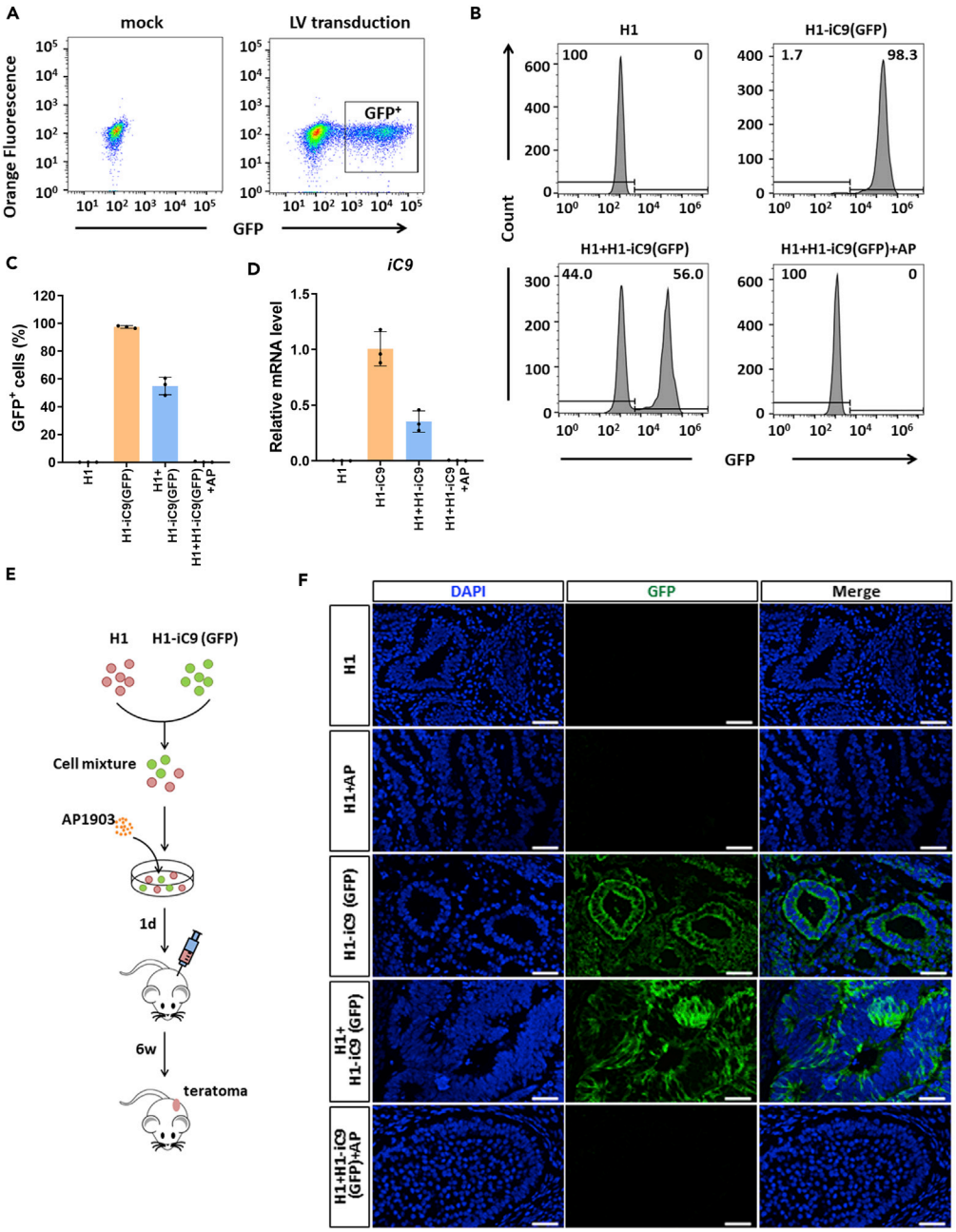

Figure 2. iC9-Expressing Cells Are Selectively Eradicated by AP1903

(A) Marking of H1-iC9 cells with GFP. Structure of the lentiviral vector containing the *GFP* gene is shown. H1-iC9 cells were transduced with the GFP vector at a multiplicity of infection of two, followed by cell sorting 48 h after transduction. GFP^+ cells were pooled and expanded.

(B and C) Flow cytometry analysis of H1 and H1-iC9(GFP) cells either alone or in mixtures with and without AP1903 treatment as indicated. (B) FACS plots present the percentage of GFP^+ cells in each group. (C) Bar graph shows mean (±s.d.) of pooled data from three independent experiments.

(D) Expression of iC9 transgene mRNA in the indicated cells. Results of three independent experiments are shown as the mean ± s.d.

(E) Experimental scheme for the teratoma formation assay. H1 and H1-iC9(GFP) cells were mixed at an equal dose and either mock treated or treated with AP1903 overnight at a concentration of 10 nM, followed by subcutaneous injection of 2×10^6 cells into NSG mice with four mice per group. Teratomas were removed six weeks after injection.

(F) Representative immunofluorescence staining of GFP in teratoma sections derived from indicated cells. Scale bar = 50 μm.

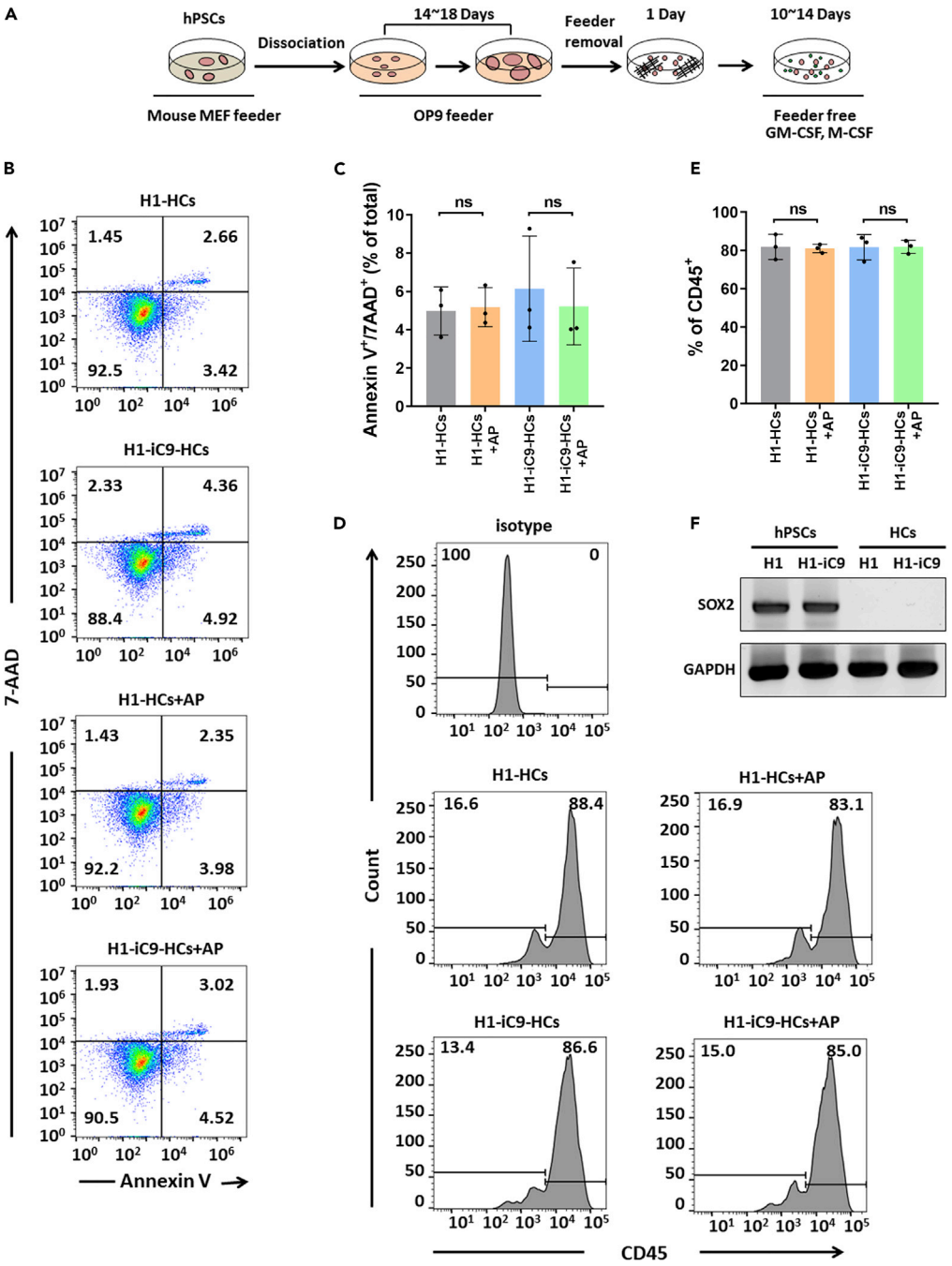

Figure 3. Effect of AP1903 Treatment on H1-iC9-Derived Hematopoietic Cells

(A) Scheme of differentiation from hPSCs to hematopoietic cells.

(B and C) Flow cytometry analysis of apoptosis of hematopoietic cells derived from H1 and H1-iC9 cells with AP1903 treatment. Representative FACS profiles (B) and the bar graph showing percentage of apoptotic cells from three independent experiments (C) were shown and presented as the mean ± s.d. ns: p value not significant.

(D and E) The fraction of $CD45^+$ hematopoietic cells derived from H1 and H1-iC9 differentiation was not affected by AP1903 treatment. Mock- or AP1903-treated hematopoietic cells were analyzed by flow cytometry. FACS plots (D) and bar graph that represents the frequency of $CD45^+$ (E) were shown and presented as the mean ± s.d. (N = 3 independent experiments) ns: not statistically significant.

(F) Semi-quantitative RT-PCR analysis of the *SOX2* transcript in undifferentiated H1 and H1-iC9 cells as well as in the hematopoietic populations derived from these two cell lines.

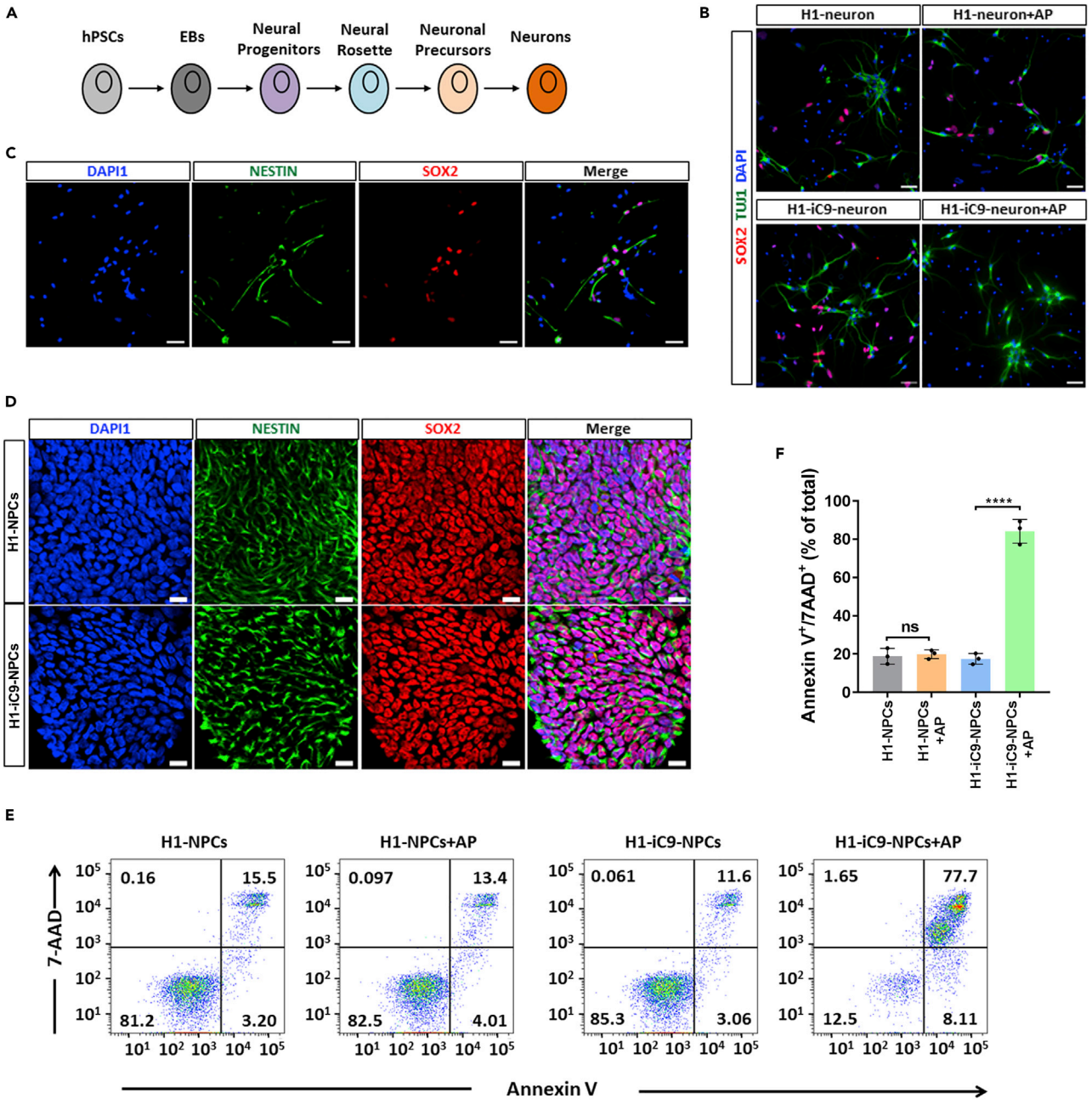

Figure 4. Effect of AP1903 Treatment on H1-iC9-Derived Neuronal Cells

(A) Scheme of neuron differentiation from hPSCs.

(B and C) Representative immunofluorescence staining of SOX2/TUJ1 (B) and SOX2/NESTIN (C) in mock- and AP1903-treated neuronal cultures derived from H1 and H1-iC9 cells. Scale bar = 50 μm.

(D) Representative immunofluorescence staining of Nestin and SOX2 in NPCs derived from H1 and H1-iC9 cells. Scale bar = 50 μm.

(E) Representative of flow cytometry analysis of cell apoptosis after overnight treatment of H1 and H1-iC9-derived NPCs with AP1903.

(F) Quantification of the apoptotic cell fraction from three independent experiments. Bars indicate the mean ± s.d., ****$p < 0.0001$, ns: not statistically significant.

undetectable in the NPC culture in contrast to readily detectable *SOX2*, indicating highly efficient differentiation (Figure S7). AP1903 treatment led to a significant loss of these cells derived from H1-iC9 cells but not those from H1 cells (Figures 4E and 4F). Thus, this suicide system permits selective removal of $SOX2^+$ cells without affecting terminal differentiated neurons in the same culture.

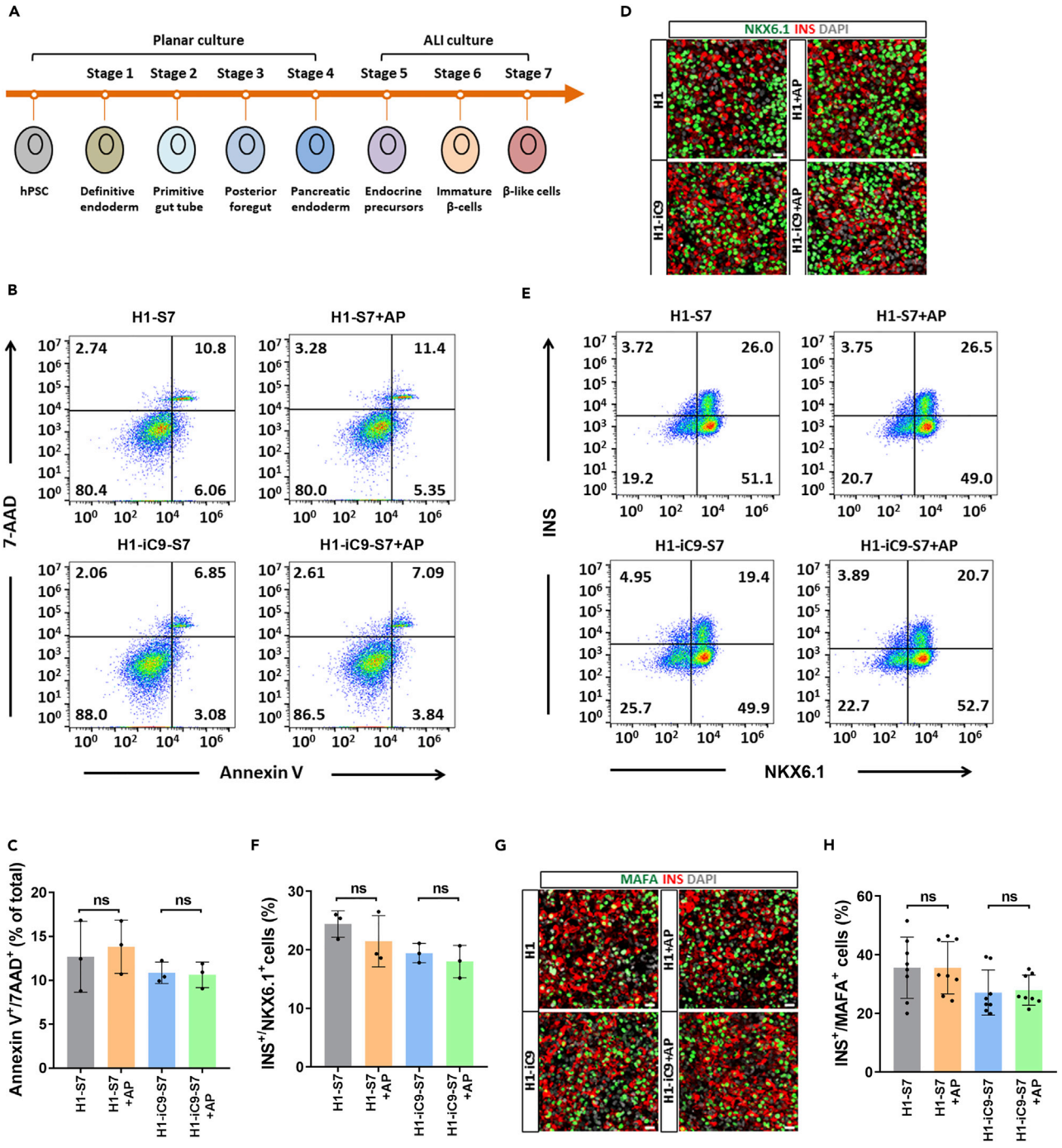

Figure 5. H1-iC9-Derived Beta-like Cells Are Resistant to AP1903 Treatment

(A) Seven-stage differentiation of hPSCs into beta-like cells. Cells were grown in monolayer from stage 1 to stage 4 and in an air-liquid (ALI) interphase from stage 5 to stage 7.

(B) Flow cytometry analysis of the apoptotic cells in the S7 population derived from H1 and H1-iC9 cells after overnight AP1903 treatment.

(C) Quantification of the fraction of Annexin $V^+/7AAD^+$ apoptotic cells from three independent experiments. Data present the mean frequency ±s.d., ns: not statistically significant.

(D) Representative immunofluorescence staining of $NKX6.1^+/INS^+$ cells in the S7 population derived from H1 and H1-iC9 cells with and without AP1903 treatment.

(E) Flow cytometry analysis of $NKX6.1^+$ and INS^+ cells in H1 or H1-iC9-derived S7 cells with and without AP1903 treatment.

Figure 5. *Continued*

(F) Quantification of NKX6.1$^+$/INS$^+$ cell proportion from three independent experiments. Data indicate the mean ± s.d., ns: not statistically significant.

(G) Representative immunofluorescence staining of MAFA$^+$ and INS$^+$ cells.

(H) Quantification of the fraction of MAFA$^+$/INS$^+$ beta-like cells. Bars represent the mean ± s.d. from three independent experiments, ns: not statistically significant. MAFA$^+$/INS$^+$ beta-like cells were counted in eight randomly picked fields. Scale bar = 20 μm.

Resistance of H1-iC9-Derived Beta-like Cells to AP1903 Treatment

To evaluate the effect of iC9 on hPSC-derived endocrine lineages, we adopted a seven-stage differentiation protocol to generate pancreatic beta-like cells from H1 and H1-iC9 cells (Figure 5A) (Rezania et al., 2014). AP1903 treatment did not noticeably alter the viability of differentiated cells derived from either H1 or H1-iC9 in stage 4 (S4) or S7 (Figures 5B, 5C, and S8A). Examination of AP1903-treated S4 cells revealed no major change in the fraction of pancreatic progenitor cells marked by PDX1 or NKX6.1 expression (Figure S8B). More importantly, the fractions of NKX6.1$^+$/Insulin$^+$ cells and MAFA$^+$/Insulin$^+$ cells considered to be more mature beta cells in S7 were not affected by AP1903 treatment (Figures 5D–5H). Thus, H1- and H1-iC9-derived pancreatic progenitor cells and beta-like cells are resistant to AP1903 treatment, presumably due to down-regulation of SOX2 expression.

However, real-time PCR of the *SOX2* transcript showed that although *SOX2* expression was significantly down-regulated in S1 and S2 during pancreatic differentiation of H1 and H1-iC9 cells, it was reactivated in S3, peaked in S4, and persisted at lower levels in S7 (Figure 6A). Flow cytometry analysis of S7 cells showed SOX2$^+$ cells in both H1- and H1-iC9-derived cultures, and AP1903 treatment did not lead to the elimination of the SOX2$^+$ cells (Figures 6B and 6C). Immunofluorescence staining of insulin and SOX2 confirmed that these SOX2$^+$ cells were not beta-like cells (Figure 6D). The *iC9* transcript displayed a similar pattern of changes during differentiation relative to the *SOX2* transcript (Figure S9). In consistent with the transcript, iC9 protein was detected in SOX2$^+$ cells at S7, indicating that transgene was not shutdown (Figure 6E). To ensure that AP1903 resistance of these SOX2$^+$ cells is not due to iC9 mutation, we sequenced the *iC9* transcript in the S7 culture and found no changes in its sequence (data not shown). To determine whether these SOX2$^+$ cells are contaminating undifferentiated cells, we performed real-time PCR of S7 cells and found no trace of *OCT4* and *NANOG* transcripts (Figure 6F). Immunofluorescence staining and FACS analysis confirmed that SOX2$^+$ cells in the S7 population failed to co-express OCT4 or NANOG but co-expressed definitive endoderm marker FOXA2 (Figures 6G and S10). Moreover, mRNA level of FOXA2 was dramatically increased in S4 and S7 cells compared with undifferentiated cells, indicating the generation of definitive endoderm cells upon differentiation (Figure S11). It is well known that the pluripotency marker *SOX2* reemerges as an anterior foregut marker (Green et al., 2011). We thus analyzed transcripts of other anterior foregut markers including *HOXA1*, *HOXA2,* and *PAX9*. In contrast to *SOX2* gene, which was highly expressed in undifferentiated cells, expression of all these markers was undetectable in both H1 and H1-iC9 cells. *PAX9* expression remained undetectable upon differentiation (data not shown). By contrast, *HOXA1* and *HOXA2* expression was markedly up-regulated in S4 cells and down-regulated in S7 cells (Figure S11). Collectively, these data suggested the possibility that SOX2$^+$ cells reappeared during beta-like cell differentiation were endoderm-derived anterior foregut cells.

Previous studies showed that the Caspase 9 signaling cascade plays a role in amplifying mitochondrial disruption through cleavage of anti-apoptotic BCL-2 family proteins, and expression of a cleavage-resistant BCL-2 mutant or overexpression of wild-type BCL-2 inhibited Caspase-9-mediated apoptosis (Chen et al., 2007; Yang et al., 1997). Since BCL-2 expression was shown to be up-regulated upon differentiation of mouse ESCs and hPSCs (LeBlanc et al., 2018; Lee et al., 2013), we carried out Western blot analysis to detect BCL-2 expression in H1-iC9 and H1-iC9-derived S7 cells. As shown in Figure 6H, the level of BCL-2 in the S7 population was strongly up-regulated compared with that in undifferentiated cells. This result raises the possibility that up-regulation of BCL-2 may play a role in conferring the resistance of SOX2$^+$ cells in S7 to AP1903 treatment.

Selective Removal of Undifferentiated H1-iC9 Cells from the S7 Beta-like Cell Population

To determine whether contaminating undifferentiated stem cells can be removed from the S7 cell population, undifferentiated H1-iC9 cells were spiked into H1-iC9-derived S7 culture followed by AP1903 treatment. Undifferentiated H1-iC9 cells were identified by the expression of OCT4, a stem-cell-specific marker. As shown in Figure 6I, AP1903 treatment selectively eliminated undifferentiated H1-iC9 cells without affecting the viability of OCT4$^-$ S7 cells. These data also suggested that the S7 culture condition or the

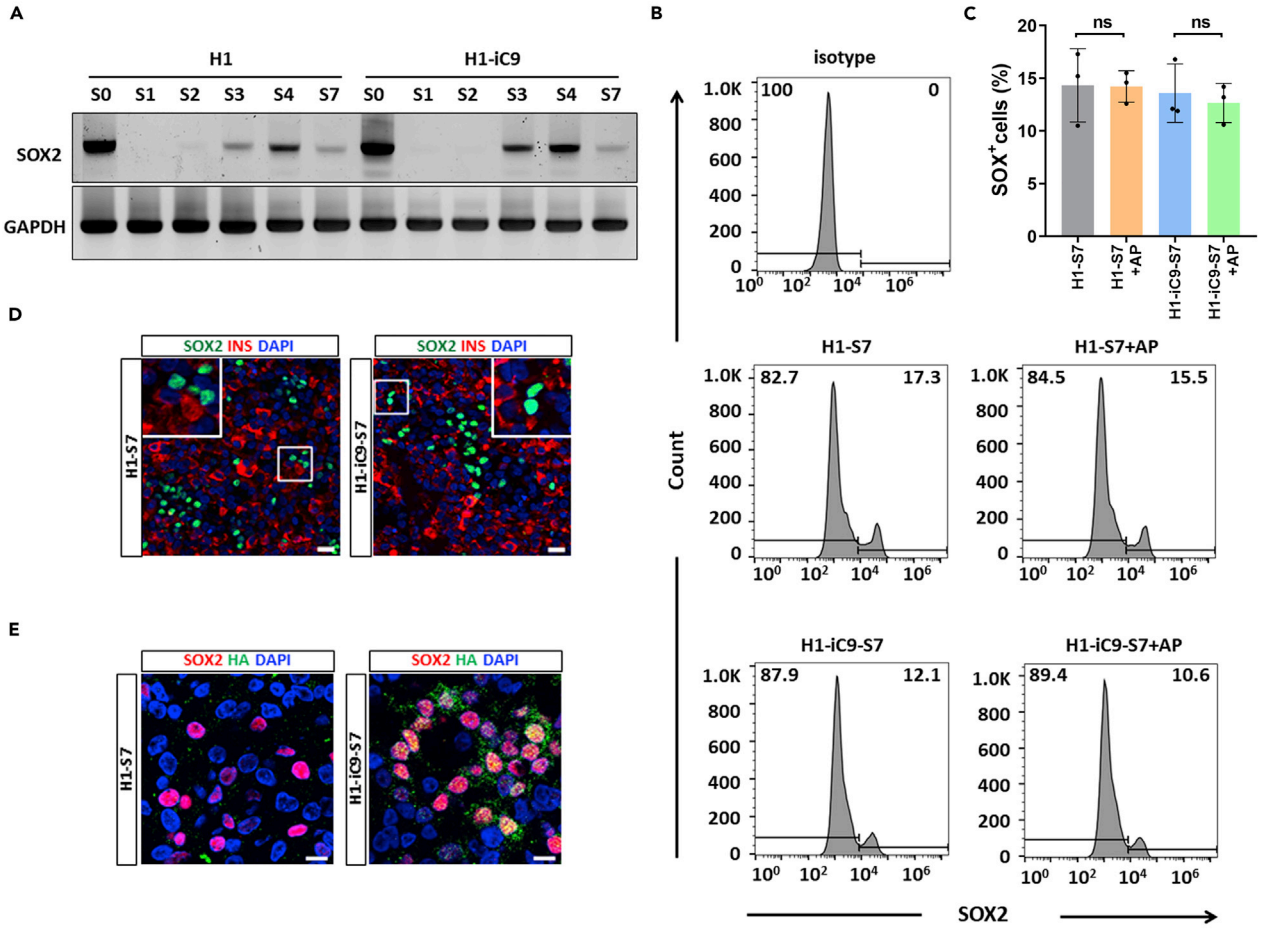
A
H1
H1-iC9
S0 S1 S2 S3 S4 S7 S0 S1 S2 S3 S4 S7
SOX2
GAPDH
B
isotype
100
0
1.0K
800
600
400
200
0
10^0 10^2 10^4 10^6
C
ns
ns
20
15
10
5
0
SOX+cells (%)
H1-S7
H1-S7 +AP
H1-iC9-S7
H1-iC9-S7 +AP
D
SOX2 INS DAPI
SOX2 INS DAPI
H1-S7
H1-iC9-S7
H1-S7
H1-S7+AP
82.7
17.3
84.5
15.5
Count
E
SOX2 HA DAPI
SOX2 HA DAPI
H1-S7
H1-iC9-S7
H1-iC9-S7
H1-iC9-S7+AP
87.9
12.1
89.4
10.6
SOX2
F
H1
H1-iC9
S0 S7 S0 S7
NANOG
OCT4
SOX2
GAPDH
G
SOX2
FOXA2
SOX2 FOXA2
H
S0 S7 KDa
BCL2
GAPDH
-26
-34
I
Count
500
400
300
200
100
0
10^3 10^4 10^5
isotype
S0
S7
S0+S7
S0+S7+AP

Figure 6. SOX2$^+$ Cells in the S7 Population Remain Viable after AP1903 Treatment Are Not Undifferentiated Stem Cells

(A) Reactivation of *SOX2* expression during H1 and H1-iC9 cell differentiation into beta-like cells. Semi-quantitative RT-PCR was carried out using total RNAs isolated from the indicated differentiation stages as defined by Rezania et al. (Rezania et al., 2014).

(B and C) Resistance to AP1903 treatment of SOX2$^+$ cells in the S7 population. Flow cytometry analysis of the SOX2$^+$ expression in mock- and AP1903-treated S7 populations derived from H1 and H1-iC9 cells and quantification of SOX2$^+$ proportion from B. Bars present the mean ± s.d. of three independent experiments. ns: not statistically significant.

(D) Representative immunofluorescence staining of SOX2 and insulin in S7 cells. Scale bar = 20 μm.

(E) Co-staining of SOX2 and the HA tag in iC9 in the S7 population derived from H1 and H1-iC9 cells. Cell nuclei were counterstained with DAPI. Scale bar = 10 μm.

(F) Semi-quantitative RT-PCR analysis of *NANOG*, *OCT4*, and *SOX2* transcripts in undifferentiated (S0) and the Stage 7 (S7) populations derived from H1 and H1-iC9 cells.

(G) Representative immunofluorescence staining of SOX2 and FOXA2 in the H1-iC9-derived S7 population. Scale bar = 20 μm.

(H) Western blot analysis of BCL2 expression in S0 and S7 populations derived from H1-iC9 cells.

(I) Selective eradication of undifferentiated H1-iC9 cells spiked into H1-iC9-derived S7 population. Undifferentiated H1-iC9 cells spiked into H1-iC9-derived S7 population were treated with 10 nM AP1903 overnight. The resulting cell mixture was stained for OCT4 and analyzed by flow cytometry.

cell microenvironment was not inhibitory to AP1903-induced cell apoptosis. Based on these results, we concluded that the iC9 suicide system could be applied to selectively eliminate contaminating undifferentiated hPSCs without affecting differentiated beta-like cells.

DISCUSSION

The genetic manipulation we carried out in the *SOX2* locus did not affect the stemness of H1-iC9 cells, as they continued to express OCT4, SOX2, and NANOG at a similar level as the parental H1 cells (Figure 6F). The pluripotency of H1-iC9 cells was not affected neither as shown by their ability to form teratomas and to differentiate into hematopoietic cells, neurons, and pancreatic beta-like cells at similar efficiencies as H1 parental cells. Thus, ectopic expression of the *iC9* gene product causes little adverse effect on the ability of self renewal and pluripotency of H1 cells. This approach therefore provides a platform to establish suicide-gene-containing hPSCs to facilitate their safe application in cell-based therapy.

In the current study, we chose the *SOX2* locus for suicide gene insertion because of minimum potential off-target effect compared with the *OCT4* and *NANOG* loci. By contrast, multiple genomic sites exhibit sequence homology with the on-target sites at the *OCT4* and *NANOG* loci. It is therefore difficult to design sgRNAs that specifically cleave only the on-target sequence at these two loci. Zhu et al. previously reported the design of a sgRNA for in-frame insertion of fluorescence marker genes into the *OCT4* locus in hESCs (Zhu et al., 2015). All potential *OCT4* off-target sequences identified in our study except the one on chromosome 3 exhibit identical sequences to the *OCT4* on-target sequence reported by Zhu et al. (Zhu et al., 2015). It is highly likely that the sgRNA they designed would generate double-strand breaks (DSBs) at these off-target sites, increasing the likelihood of indel formation or chromosome translocation. To reduce the risk of off-target cleavage, we used Cas9 nickase together with two sgRNAs targeting the site at the *SOX2* locus for *iC9* gene insertion. We sequenced the potential off-target site on chromosome 8 and the top five predicted off-target sites for each sgRNA in H1-iC9 cells and detected no sequence changes (Table S1), confirming the safety of using such a strategy to insert the suicide gene into a well-characterized stem cell locus.

Our result showed that although *SOX2* expression was initially down-regulated during H1 differentiation into pancreatic beta-like cells, it was reactivated at stage 3 during posterior foregut formation, and SOX2$^+$ cells persisted into S7 when beta-like cells emerged (Figure 6A). The emergence of these cells was not an artifact caused by gene editing, as they also existed in H1-derived S7 cells. In addition, our data showed that these SOX2$^+$ cells were not undifferentiated stem cells or beta-like cells. SOX2 is strongly expressed in undifferentiated stem cells and becomes down-regulated during endoderm commitment. SOX2 expression reappears upon anterior-posterior patterning of the definitive endoderm to form foregut and persists in anterior foregut (Que et al., 2007). The co-expression of SOX2 and FOXA2 (Figure 6G) as well as the reactivation of *HOXA1* and *HOXA2* (Figure S11) suggested that SOX2$^+$ cells generated during beta cell differentiation were anterior foregut endoderm cells. These results were consistent with the RNA-seq analysis for beta-cell differentiation published recently by Melton group (Veres et al., 2019). The production of these SOX2$^+$ cells also reflects the fact that current differentiation protocols produced mixed cell population including small portion of non-endocrine cells (Veres et al., 2019). Although the differentiation protocol we used favors the formation of posterior foregut in S3 (Rezania et al., 2014), some anterior foregut

cells could conceivably be generated by some small molecules. Our protocol includes bone morphogenetic protein (BMP) inhibitor LDN in S3 and S4 during differentiation. Inhibition of BMP signaling after specification of definitive endoderm from hPSCs has been shown to reactivate SOX2 expression in derived anterior foregut cells (Davenport et al., 2016; Green et al., 2011).

The finding that S7 cells expressed high levels of the anti-apoptotic BCL-2 protein could partially explain AP1903 resistance of $SOX2^+$ cells. BCL-2 family proteins regulate the intrinsic apoptotic pathway by blocking the mitochondrial disruption that triggers the activation of Caspase 9 (Youle and Strasser, 2008). Although BCL-2 presumably acts upstream of Caspase, several studies showed that the Caspase 9 signaling cascade also induces mitochondrial disruption through the cleavage of BCL-2 (Chen et al., 2007; Cheng et al., 1997), thereby amplifying the intrinsic apoptotic pathway. High levels of BCL-2 protein may block this positive feedback loop and render the cells resistant to apoptosis. Down-regulation of BCL-2 or related anti-apoptotic proteins in the S7 culture with siRNA or shRNA may ultimately confirm the role of these proteins on the resistance to AP1903 treatment.

The use of various suicide gene systems to eliminate undifferentiated PSCs and prevent teratoma formation has been reported in several studies. For the iC9 suicide system, PSCs from different species transduced with lentivirus expressing *iC9* could be effectively eradicated by AP 1903 (Wu et al., 2014; Yagyu et al., 2015). Another widely used suicide gene based on the HSV-TK/GCV induces cell killing by disruption of DNA synthesis and inhibition of cell proliferation (Cheng et al., 2012; Schuldiner et al., 2003). More recently, Qadir et al reported a new strategy by co-introduction of two suicide genes encoding HSV-TK and *Escherichia coli* nitroreductase (NTR) (Qadir et al., 2019). The strategy establishes a double-safe mechanism to ensure the eradication of any potential tumorigenic escapee while preserving differentiated cells through Cre recombination. An alternative approach using virus-like particles (VLPs) labeling with antibodies against a surface marker of hPSCs, SSEA-5, to deliver cytosine deaminase (CD) was designed to eliminate dividing cells with 5-fluorocytosine (5-FC) (Rampoldi et al., 2018). This strategy avoids the biosafety issue raised by transgenetic modification, but the efficiency of targeting undifferentiated cells remains to be tested. For example, because 3D culture systems are widely used in various cell differentiation protocols, whether VLPs can effectively introduce a toxic product into the core of cell aggregates from a 3D culture is unknown. To achieve reliable expression of suicide gene, instead of random transgene insertion mediated by a virus, site-specific insertion of a suicide gene by genome editing was applied. Ou et al. attempted to insert the HSV-TK gene into the *OCT4* locus in hPSCs by zinc finger nucleases (ZFN) (Ou et al., 2013). However, the genetically modified hPSC clones were not sensitive to GCV and high rate of off-target insertion was also observed in their study. Our results that a selectable marker can interfere with the expression of the adjacent suicide gene and the detection of multiple genomic loci exhibiting similar or identical sequence as the *OCT4* locus could provide possible explanations for Qu et al.'s observations. During the submission of the current work, Liang et al. reported a strategy of in-frame insertion of the *HSV-TK* gene into the cyclin-dependent kinase 1 (*CDK1*) locus in hESC lines (Liang et al., 2018). Because CDK1 is not expressed in non-dividing cells (Diril et al., 2012; Santamaria et al., 2007), their strategy ensures selective expression of the *HSV-TK* gene only in dividing cells, which can be eradicated by GCV. Although both the TK and our iC9 system are drug inducible, they use distinc mechanisms to induce cell death. The two systems may therefore complement each other to improve the safety of using stem cell-derived products in cell-based therapies.

In summary, our data demonstrate the feasibility of using an endogenous locus to modulate the expression of the *iC9* gene for selective eradication of undifferentiated hPSCs. The three lineages we tested, including hematopoietic cells, neurons, and pancreatic beta-like cells, are potential candidates for clinical applications. AP1903 treatment of these cell lineages did not seem to affect cell viability or lineage commitment. Although residue $SOX2^+$ cells remained in the derived S7 pancreatic beta-like cell population, they were not undifferentiated hPSCs and thus had no potential to form teratomas. This is consistent with the lack of teratoma formation in immunodeficient mice transplanted with the S7 cells from this differentiation protocol (Rezania et al., 2014). The strategy described here should therefore provide a layer of safety control to reduce the risk of teratoma from transplanted hPSC-derived cell products.

Limitations of the Study

In this study, *SOX2* was used as the locus for insertion of a suicide gene due to the reduced off-target effect generated by CRISPR-Cas9 when compared with other two stem cell loci, *OCT4* and *NANOG*. However, SOX2 is not only an important transcription regulator for stem cell pluripotency but is also involved in differentiation of neural progenitor cells and patterning of the foregut endoderm. Therefore,

although we have demonstrated that this system can be applied in three clinically relevant hPSC-derived cell products, it is not applicable in cell types such as neuronal progenitor cells and anterior foregut cells that also express SOX2 at high levels. As shown in Figure 4E, neural progenitor cells rapidly became apoptotic upon AP1903 treatment. Finding a locus exclusively activated in hPSCs but not in these cells would circumvent this problem. In addition, our system is designed specifically to eradicate undifferentiated stem cells before transplantation to minimize the risk of teratoma formation. However, this strategy may not be sufficient to eliminate already formed tumors derived from the transplanted cell products due to the down-regulation of SOX2. The *iC9* system and other *TK* gene-based strategies may therefore complement each other to improve the safety of stem-cell-derived products in transplantation therapy.

METHODS

All methods can be found in the accompanying Transparent Methods supplemental file.

SUPPLEMENTAL INFORMATION

Supplemental Information can be found online at https://doi.org/10.1016/j.isci.2019.11.038.

ACKNOWLEDGMENTS

This work is supported by a grant from Wanek Innovation Program. Y.L. is support by the Project of International Cooperation and Exchanges of China, China [81520108002]. Research reported in this publication included work performed in the Animal Tumor Models Program, Pathology Solid Tumor Core, Integrative Genomics Core, and Analytical Cytometry Core supported by the National Cancer Institute of the National Institutes of Health, United States under award number P30CA033572. The content is solely the responsibility of the authors and does not necessarily represent the official views of the National Institutes of Health.

AUTHOR CONTRIBUTIONS

Y.W., F.K., and J.K.Y. conceived and designed experiments; Y.W., T.C., and Y.L. performed experiments; Y.W., F.K., H.H., and J.K.Y. provided data analysis and interpretation; Y.W. and J.K.Y. wrote the manuscript.

DECLARATION OF INTERESTS

The authors indicated no competing interests.

Received: May 16, 2019
Revised: October 13, 2019
Accepted: November 19, 2019
Published: December 20, 2019

REFERENCES

Balboa, D., Weltner, J., Novik, Y., Eurola, S., Wartiovaara, K., and Otonkoski, T. (2017). Generation of an OCT4 reporter human induced pluripotent stem cell line using CRISPR/SpCas9. Stem Cell Res. *23*, 105–108.

Boer, B., Kopp, J., Mallanna, S., Desler, M., Chakravarthy, H., Wilder, P.J., Bernadt, C., and Rizzino, A. (2007). Elevating the levels of Sox2 in embryonal carcinoma cells and embryonic stem cells inhibits the expression of Sox2:Oct-3/4 target genes. Nucleic Acids Res. *35*, 1773–1786.

Bokhoven, M., Stephen, S.L., Knight, S., Gevers, E.F., Robinson, I.C., Takeuchi, Y., and Collins, M.K. (2009). Insertional gene activation by lentiviral and gammaretroviral vectors. J. Virol. *83*, 283–294.

Bonini, C., Ferrari, G., Verzeletti, S., Servida, P., Zappone, E., Ruggieri, L., Ponzoni, M., Rossini, S., Mavilio, F., Traversari, C., et al. (1997). HSV-TK gene transfer into donor lymphocytes for control of allogeneic graft-versus-leukemia. Science *276*, 1719–1724.

Caserta, T.M., Smith, A.N., Gultice, A.D., Reedy, M.A., and Brown, T.L. (2003). Q-VD-OPh, a broad spectrum caspase inhibitor with potent antiapoptotic properties. Apoptosis *8*, 345–352.

Chen, M., Guerrero, A.D., Huang, L., Shabier, Z., Pan, M., Tan, T.H., and Wang, J. (2007). Caspase-9-induced mitochondrial disruption through cleavage of anti-apoptotic BCL-2 family members. J. Biol. Chem. *282*, 33888–33895.

Cheng, E.H., Kirsch, D.G., Clem, R.J., Ravi, R., Kastan, M.B., Bedi, A., Ueno, K., and Hardwick, J.M. (1997). Conversion of Bcl-2 to a Bax-like death effector by caspases. Science *278*, 1966–1968.

Cheng, F., Ke, Q., Chen, F., Cai, B., Gao, Y., Ye, C., Wang, D., Zhang, L., Lahn, B.T., Li, W., et al. (2012). Protecting against wayward human induced pluripotent stem cells with a suicide gene. Biomaterials *33*, 3195–3204.

Clackson, T., Yang, W., Rozamus, L.W., Hatada, M., Amara, J.F., Rollins, C.T., Stevenson, L.F., Magari, S.R., Wood, S.A., Courage, N.L., et al. (1998). Redesigning an FKBP-ligand interface to generate chemical dimerizers with novel specificity. Proc. Natl. Acad. Sci. U S A *95*, 10437–10442.

Davenport, C., Diekmann, U., Budde, I., Detering, N., and Naujok, O. (2016). Anterior-posterior patterning of definitive endoderm generated from human embryonic stem cells depends on the differential signaling of retinoic acid, Wnt-, and BMP-signaling. Stem Cells *34*, 2635–2647.

Davis, R.P., Costa, M., Grandela, C., Holland, A.M., Hatzistavrou, T., Micallef, S.J., Li, X., Goulburn, A.L., Azzola, L., Elefanty, A.G., et al. (2008). A protocol for removal of antibiotic resistance cassettes from human embryonic stem cells genetically modified by homologous

recombination or transgenesis. Nat. Protoc. *3*, 1550–1558.

Diril, M.K., Ratnacaram, C.K., Padmakumar, V.C., Du, T., Wasser, M., Coppola, V., Tessarollo, L., and Kaldis, P. (2012). Cyclin-dependent kinase 1 (Cdk1) is essential for cell division and suppression of DNA re-replication but not for liver regeneration. Proc. Natl. Acad. Sci. U S A *109*, 3826–3831.

Graham, V., Khudyakov, J., Ellis, P., and Pevny, L. (2003). SOX2 functions to maintain neural progenitor identity. Neuron *39*, 749–765.

Green, M.D., Chen, A., Nostro, M.C., d'Souza, S.L., Schaniel, C., Lemischka, I.R., Gouon-Evans, V., Keller, G., and Snoeck, H.W. (2011). Generation of anterior foregut endoderm from human embryonic and induced pluripotent stem cells. Nat. Biotechnol. *29*, 267–272.

Hentze, H., Soong, P.L., Wang, S.T., Phillips, B.W., Putti, T.C., and Dunn, N.R. (2009). Teratoma formation by human embryonic stem cells: evaluation of essential parameters for future safety studies. Stem Cell Res. *2*, 198–210.

Hockemeyer, D., Soldner, F., Beard, C., Gao, Q., Mitalipova, M., DeKelver, R.C., Katibah, G.E., Amora, R., Boydston, E.A., Zeitler, B., et al. (2009). Efficient targeting of expressed and silent genes in human ESCs and iPSCs using zinc-finger nucleases. Nat. Biotechnol. *27*, 851–857.

Klimanskaya, I., Hipp, J., Rezai, K.A., West, M., Atala, A., and Lanza, R. (2004). Derivation and comparative assessment of retinal pigment epithelium from human embryonic stem cells using transcriptomics. Cloning Stem Cells *6*, 217–245.

Kopp, J.L., Ormsbee, B.D., Desler, M., and Rizzino, A. (2008). Small increases in the level of Sox2 trigger the differentiation of mouse embryonic stem cells. Stem Cells *26*, 903–911.

Krentz, N.A., Nian, C., and Lynn, F.C. (2014). TALEN/CRISPR-mediated eGFP knock-in add-on at the OCT4 locus does not impact differentiation of human embryonic stem cells towards endoderm. PLoS One *9*, e114275.

LeBlanc, L., Lee, B.K., Yu, A.C., Kim, M., Kambhampati, A.V., Dupont, S.M., Seruggia, D., Ryu, B.U., Orkin, S.H., and Kim, J. (2018). Yap1 safeguards mouse embryonic stem cells from excessive apoptosis during differentiation. Elife *7*, e40167.

Lee, M.O., Moon, S.H., Jeong, H.C., Yi, J.Y., Lee, T.H., Shim, S.H., Rhee, Y.H., Lee, S.H., Oh, S.J., Lee, M.Y., et al. (2013). Inhibition of pluripotent stem cell-derived teratoma formation by small molecules. Proc. Natl. Acad. Sci. U S A *110*, E3281–E3290.

Li, W., and Xiang, A.P. (2013). Safeguarding clinical translation of pluripotent stem cells with suicide genes. Organogenesis *9*, 34–39.

Liang, Q., Monetti, C., Shutova, M.V., Neely, E.J., Hacibekiroglu, S., Yang, H., Kim, C., Zhang, P., Li, C., Nagy, K., et al. (2018). Linking a cell-division gene and a suicide gene to define and improve cell therapy safety. Nature *563*, 701–704.

Menasche, P., Vanneaux, V., Hagege, A., Bel, A., Cholley, B., Parouchev, A., Cacciapuoti, I., Al-Daccak, R., Benhamouda, N., Blons, H., et al. (2018). Transplantation of human embryonic stem cell-derived cardiovascular progenitors for severe ischemic Left ventricular dysfunction. J. Am. Coll. Cardiol. *71*, 429–438.

Moolten, F.L. (1986). Tumor chemosensitivity conferred by inserted herpes thymidine kinase genes: paradigm for a prospective cancer control strategy. Cancer Res. *46*, 5276–5281.

Ng, E.S., Davis, R.P., Azzola, L., Stanley, E.G., and Elefanty, A.G. (2005). Forced aggregation of defined numbers of human embryonic stem cells into embryoid bodies fosters robust, reproducible hematopoietic differentiation. Blood *106*, 1601–1603.

Ou, W., Li, P., and Reiser, J. (2013). Targeting of herpes simplex virus 1 thymidine kinase gene sequences into the OCT4 locus of human induced pluripotent stem cells. PLoS One *8*, e81131.

Pagliuca, F.W., Millman, J.R., Gurtler, M., Segel, M., Van Dervort, A., Ryu, J.H., Peterson, Q.P., Greiner, D., and Melton, D.A. (2014). Generation of functional human pancreatic beta cells in vitro. Cell *159*, 428–439.

Qadir, M.M.F., Alvarez-Cubela, S., Belle, K., Sapir, T., Messaggio, F., Johnson, K.B., Umland, O., Hardin, D., Klein, D., Perez-Alvarez, I., et al. (2019). A double fail-safe approach to prevent tumorigenesis and select pancreatic beta cells from human embryonic stem cells. Stem Cell Reports *12*, 611–623.

Que, J., Okubo, T., Goldenring, J.R., Nam, K.T., Kurotani, R., Morrisey, E.E., Taranova, O., Pevny, L.H., and Hogan, B.L. (2007). Multiple dose-dependent roles for Sox2 in the patterning and differentiation of anterior foregut endoderm. Development *134*, 2521–2531.

Rampoldi, A., Crooke, S.N., Preininger, M.K., Jha, R., Maxwell, J., Ding, L., Spearman, P., Finn, M.G., and Xu, C. (2018). Targeted elimination of tumorigenic human pluripotent stem cells using suicide-inducing virus-like particles. ACS Chem. Biol. *13*, 2329–2338.

Ran, F.A., Hsu, P.D., Lin, C.Y., Gootenberg, J.S., Konermann, S., Trevino, A.E., Scott, D.A., Inoue, A., Matoba, S., Zhang, Y., et al. (2013). Double nicking by RNA-guided CRISPR Cas9 for enhanced genome editing specificity. Cell *154*, 1380–1389.

Reardon, J.E. (1989). Herpes simplex virus type 1 and human DNA polymerase interactions with 2'-deoxyguanosine 5'-triphosphate analogues. Kinetics of incorporation into DNA and induction of inhibition. J. Biol. Chem. *264*, 19039–19044.

Rezania, A., Bruin, J.E., Arora, P., Rubin, A., Batushansky, I., Asadi, A., O'Dwyer, S., Quiskamp, N., Mojibian, M., Albrecht, T., et al. (2014). Reversal of diabetes with insulin-producing cells derived in vitro from human pluripotent stem cells. Nat. Biotechnol. *32*, 1121–1133.

Santamaria, D., Barriere, C., Cerqueira, A., Hunt, S., Tardy, C., Newton, K., Caceres, J.F., Dubus, P., Malumbres, M., and Barbacid, M. (2007). Cdk1 is sufficient to drive the mammalian cell cycle. Nature *448*, 811–815.

Schuldiner, M., Itskovitz-Eldor, J., and Benvenisty, N. (2003). Selective ablation of human embryonic stem cells expressing a "suicide" gene. Stem Cells *21*, 257–265.

Schwartz, S.D., Regillo, C.D., Lam, B.L., Eliott, D., Rosenfeld, P.J., Gregori, N.Z., Hubschman, J.P., Davis, J.L., Heilwell, G., Spirn, M., et al. (2015). Human embryonic stem cell-derived retinal pigment epithelium in patients with age-related macular degeneration and Stargardt's macular dystrophy: follow-up of two open-label phase 1/2 studies. Lancet *385*, 509–516.

Song, W.K., Park, K.M., Kim, H.J., Lee, J.H., Choi, J., Chong, S.Y., Shim, S.H., Del Priore, L.V., and Lanza, R. (2015). Treatment of macular degeneration using embryonic stem cell-derived retinal pigment epithelium: preliminary results in Asian patients. Stem Cell Reports *4*, 860–872.

Straathof, K.C., Pule, M.A., Yotnda, P., Dotti, G., Vanin, E.F., Brenner, M.K., Heslop, H.E., Spencer, D.M., and Rooney, C.M. (2005). An inducible caspase 9 safety switch for T-cell therapy. Blood *105*, 4247–4254.

Talkhabi, M., Aghdami, N., and Baharvand, H. (2016). Human cardiomyocyte generation from pluripotent stem cells: a state-of-art. Life Sci. *145*, 98–113.

Thomson, J.A., Itskovitz-Eldor, J., Shapiro, S.S., Waknitz, M.A., Swiergiel, J.J., Marshall, V.S., and Jones, J.M. (1998). Embryonic stem cell lines derived from human blastocysts. Science *282*, 1145–1147.

Veres, A., Faust, A.L., Bushnell, H.L., Engquist, E.N., Kenty, J.H., Harb, G., Poh, Y.C., Sintov, E., Gurtler, M., Pagliuca, F.W., et al. (2019). Charting cellular identity during human in vitro beta-cell differentiation. Nature *569*, 368–373.

Wichterle, H., Lieberam, I., Porter, J.A., and Jessell, T.M. (2002). Directed differentiation of embryonic stem cells into motor neurons. Cell *110*, 385–397.

Wu, C., Hong, S.G., Winkler, T., Spencer, D.M., Jares, A., Ichwan, B., Nicolae, A., Guo, V., Larochelle, A., and Dunbar, C.E. (2014). Development of an inducible caspase-9 safety switch for pluripotent stem cell-based therapies. Mol. Ther. Methods Clin. Dev. *1*, 14053.

Yagyu, S., Hoyos, V., Del Bufalo, F., and Brenner, M.K. (2015). An inducible caspase-9 suicide gene to improve the safety of therapy using human induced pluripotent stem cells. Mol. Ther. *23*, 1475–1485.

Yang, J., Liu, X., Bhalla, K., Kim, C.N., Ibrado, A.M., Cai, J., Peng, T.I., Jones, D.P., and Wang, X. (1997). Prevention of apoptosis by Bcl-2: release of cytochrome c from mitochondria blocked. Science *275*, 1129–1132.

Youle, R.J., and Strasser, A. (2008). The BCL-2 protein family: opposing activities that mediate cell death. Nat. Rev. Mol. Cell Biol. *9*, 47–59.

Zarogoulidis, P., Darwiche, K., Sakkas, A., Yarmus, L., Huang, H., Li, Q., Freitag, L., Zarogoulidis, K., and Malecki, M. (2013). Suicide gene therapy for cancer - current strategies. J. Genet. Syndr. Gene Ther. *4*, 16849.

Zhu, Z., Verma, N., Gonzalez, F., Shi, Z.D., and Huangfu, D. (2015). A CRISPR/Cas-Mediated selection-free knockin strategy in human embryonic stem cells. Stem Cell Reports *4*, 1103–1111.

ISCI, Volume *22*

Supplemental Information

Using Gene Editing to Establish a Safeguard System for Pluripotent Stem-Cell-Based Therapies

Youjun Wu, Tammy Chang, Yan Long, He Huang, Fouad Kandeel, and Jiing-Kuan Yee

SUPPLEMENTAL INFORMATION

SUPPLEMENTAL FIGURES

Figure S1

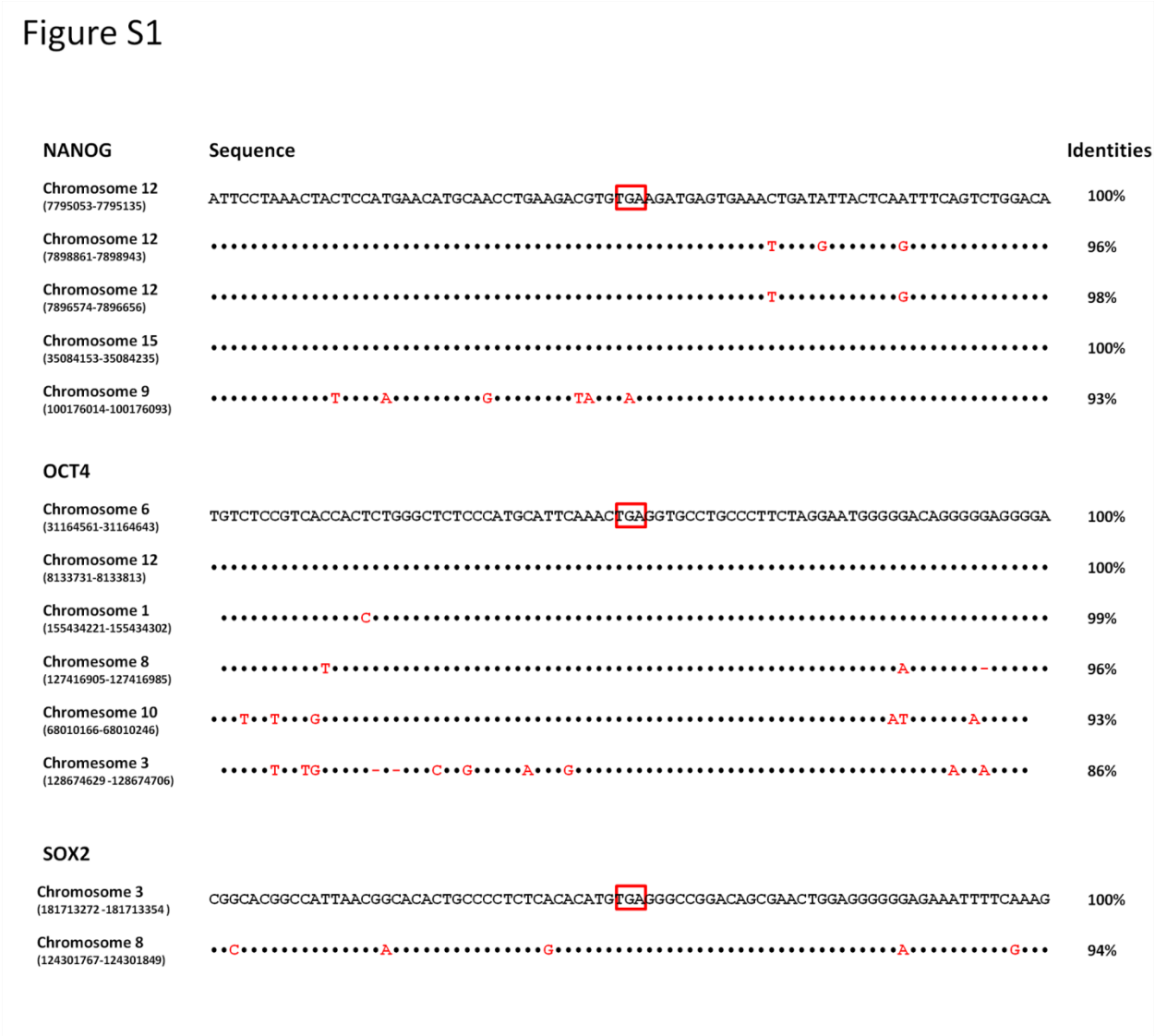

Figure S1. Chromosomal locations and sequences of the genetic loci that show sequence similarity to the *NANOG*, *OCT4,* and *SOX2* genes, related to Figure 1. Genomic sequences spanning the stop codon of the *NANOG*, *OCT4,* and *SOX2* genes are shown. Stop codons of the three genes are boxed. Mismatched nucleotides in these genetic loci are marked by red and the percentage of sequence homology is on the right.

Figure S2

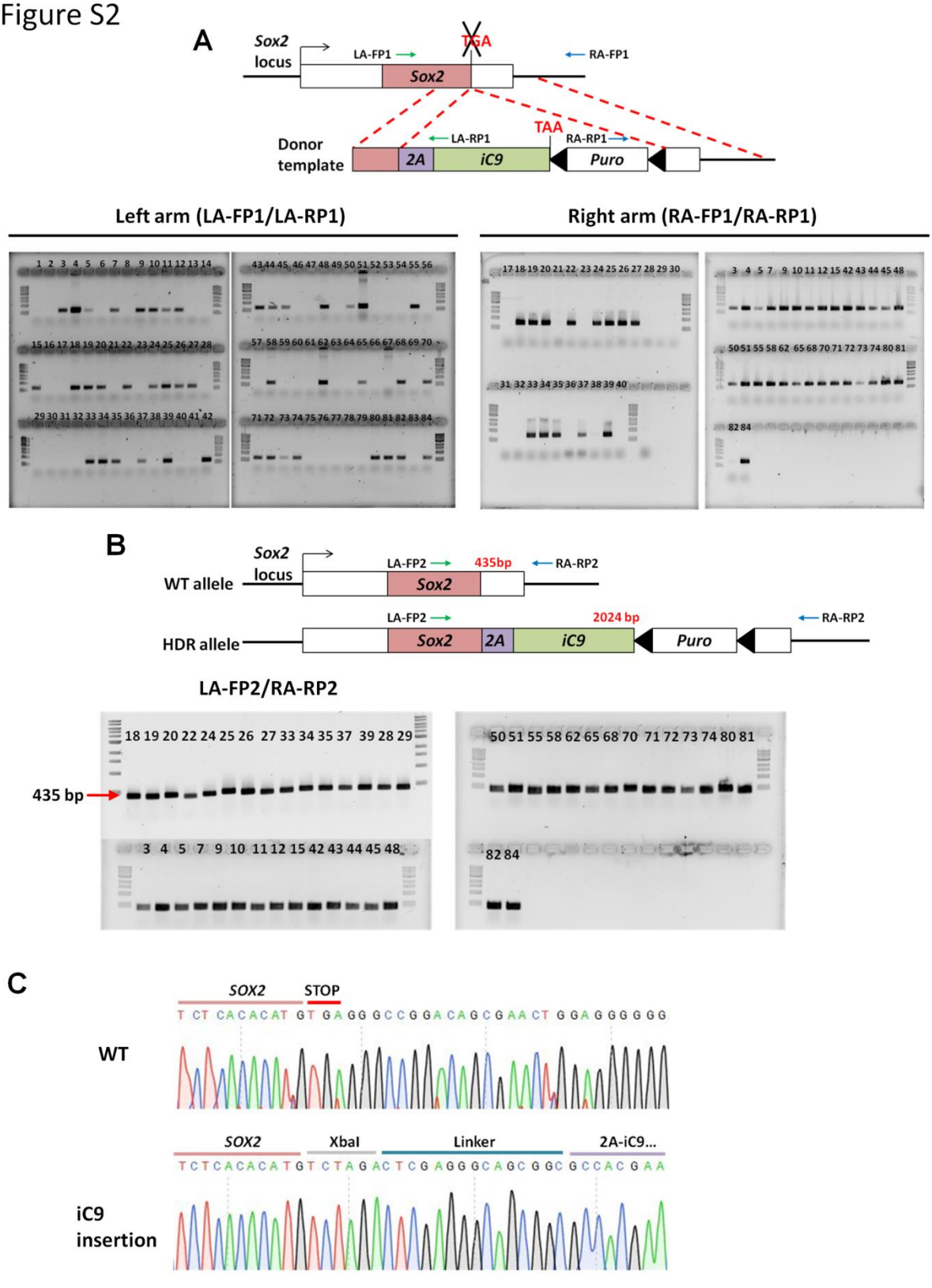
A
Sox2 locus
LA-FP1
TGA
RA-FP1
Sox2
Donor template
LA-RP1
TAA
RA-RP1
2A
iC9
Puro
Left arm (LA-FP1/LA-RP1)
Right arm (RA-FP1/RA-RP1)
B
WT allele
LA-FP2
435bp
RA-RP2
HDR allele
2024 bp
LA-FP2/RA-RP2
435 bp
C
SOX2
STOP
T CT CA CA CA T GT GA GG GC CG GA CA GC GA A CT GG A GG GG GG
WT
XbaI
Linker
2A-iC9...
T CT CA CA CA T GT CT A G A CT CG A GG GC A GC GG C GC CA C G A A
iC9 insertion

Figure S2. Establishment of the H1-iC9-pur clone, related to Figure 1. (A) Screening of H1 clones containing insertion of the *iC9* gene into the *SOX2* locus. Top: scheme for clone screening by genomic PCR. Two PCR primer pairs (green and blue arrows) and their sequences are listed in Table S2. Black arrowhead denotes the loxP site. Bottom: screening results from genomic PCR using the indicated primer pair. (B) Analysis of the positive clones identified in (A) for mono- and bi-allelic insertion of the *iC9* gene. Top: scheme for clone screening by genomic PCR. Primer pair used (green and blue arrows) and sequences are listed in Table S2. Bottom: screening results from genomic PCR using the indicated primer pair. Result indicates that all positive clones identified in (A) have a mono-allelic *iC9* gene insertion. (C) Sequence analysis of the two *SOX2* alleles near the stop codon of H1-iC9-pur cells.

Figure S3

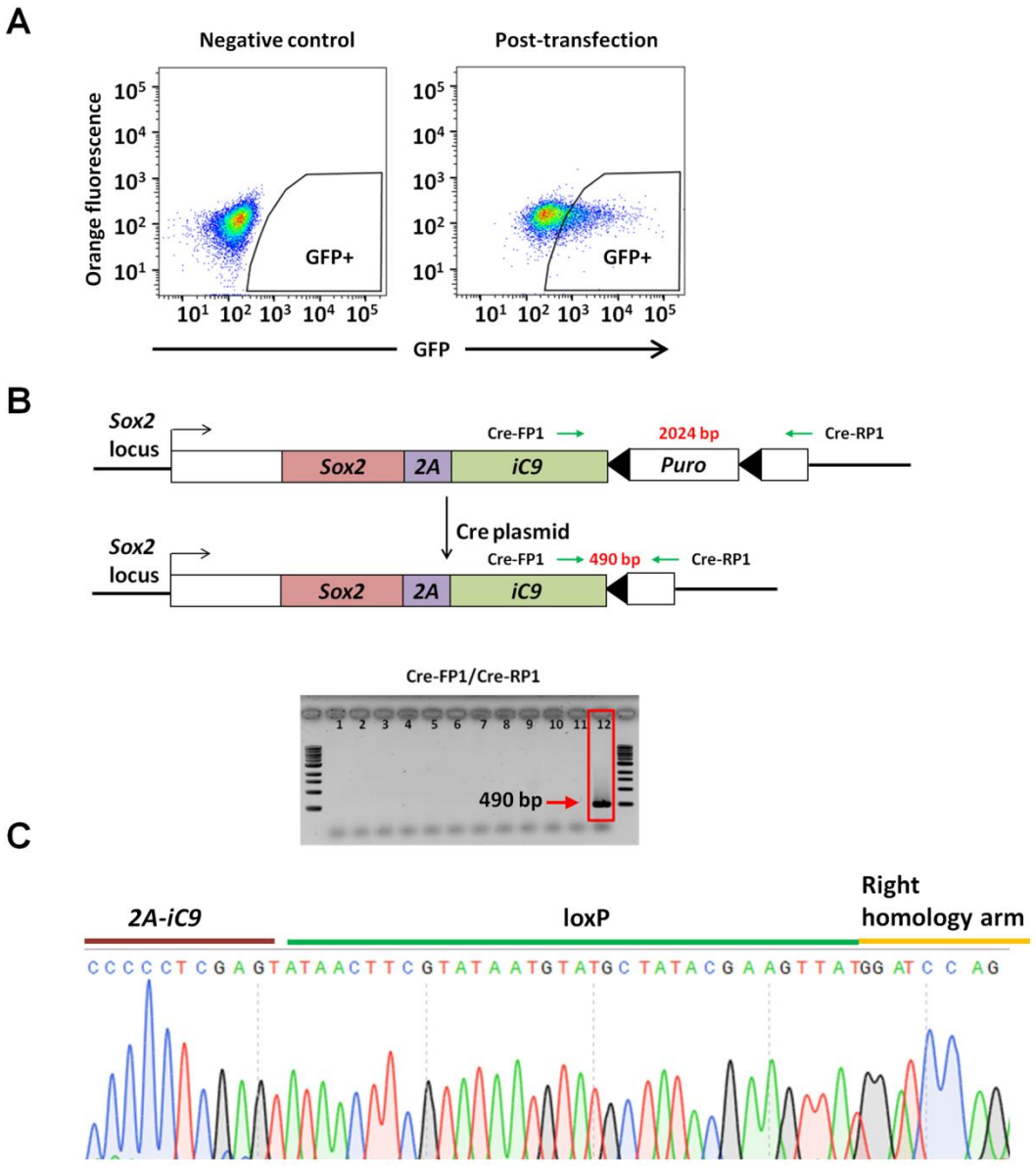

Figure S3. Isolation of the H1-iC9 clones, related to Figure 1. (A) Cell sorting of H1-iC9-pur cells co-transfected with pBS185 and pmaxGFP^{TM}. GFP^{+} cells were sorted 48 h after transfection and plated for clone isolation. (B) Isolation of the H1-iC9 clones. Top: scheme for genomic PCR screening to identify clones with the deletion of the puromycin-resistant gene. Positions of the PCR primers are indicated, and their sequences are listed in Table S2. Clones

without successful deletion of the puromycin-resistant gene are not expected to exhibit a PCR product due to the large fragment size. Bottom: A representative gel of genomic PCR result. The positive clone indicated by a red box had the expected deletion of the puromycin-resistant gene. (C) Sequence analysis of the allele containing the *iC9* gene in H1-iC9 cells confirmed deletion of the puromycin-resistant gene.

Figure S4

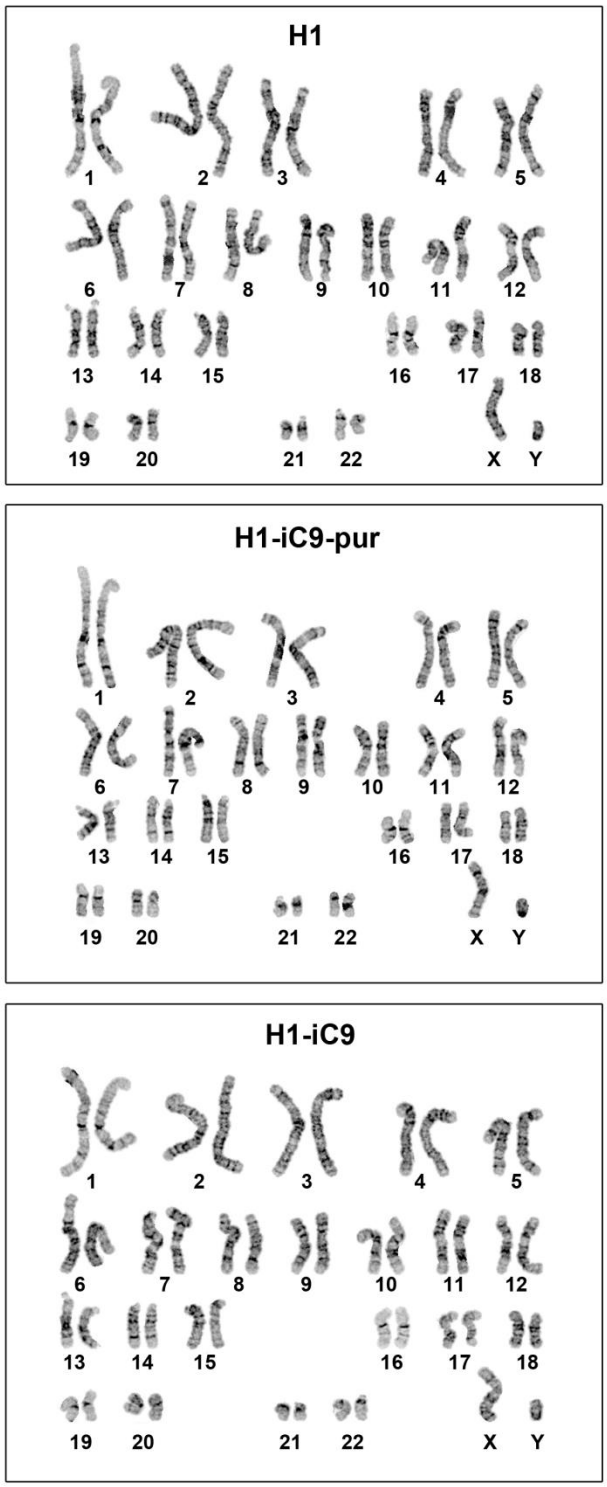

Figure S4. Karyotype analysis of H1, H1-iC9-pur and H1-iC9 cell lines, related to Figure 1.

Figure S5

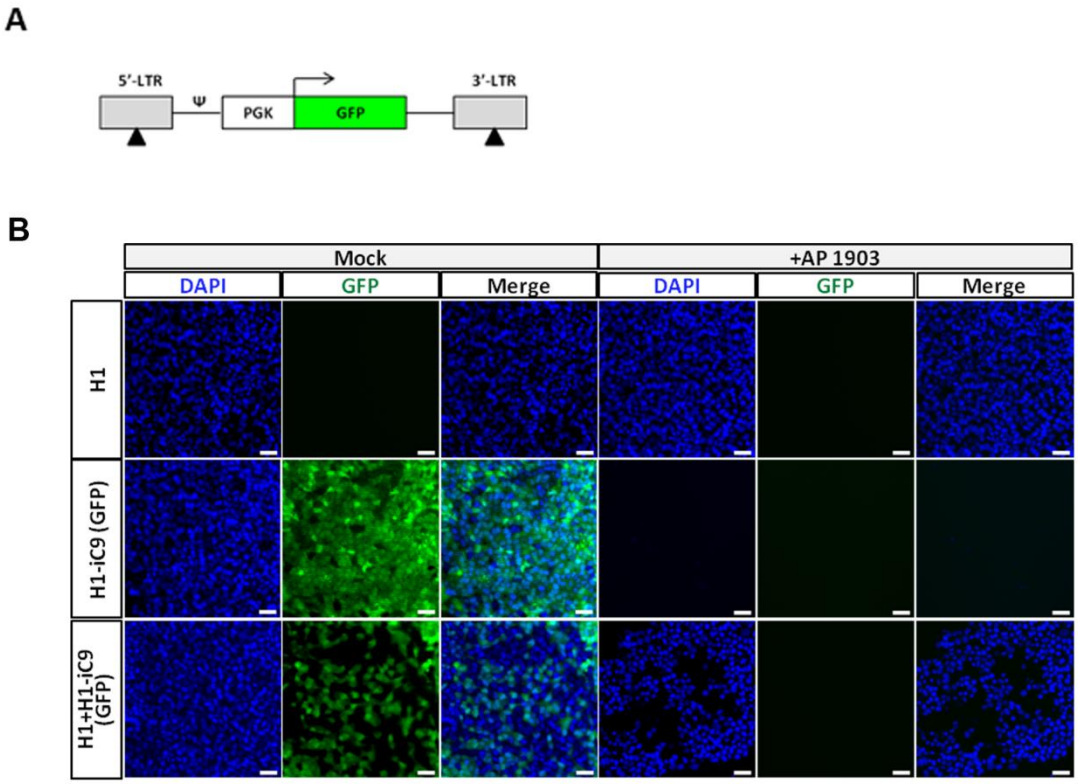

Figure S5. Selective eradication of H1-iC9 cells by AP1903 *in vitro,* related to Figure 2. (A) Marking of H1-iC9 cells with GFP. Structure of the lentiviral vector containing the *GFP* gene is shown. H1-iC9 cells were transduced with the GFP vector at a multiplicity of infection of 2, followed by cell sorting 48 h after transduction. GFP^+ cells were pooled and expanded. (B) H1 and H1-iC9(GFP) cells were either cultured alone or mixed in a 1:1 ratio. Each cell population was either mock treated or treated with 10 nM AP1903 overnight, and cell images were taken by fluorescence microscopy. The result indicates that AP1903 treatment selectively eradicates H1-iC9(GFP) cells in a mixed cell population containing both H1 and H1-iC9(GFP) cells. Scale bar = 50 µm.

Figure S6

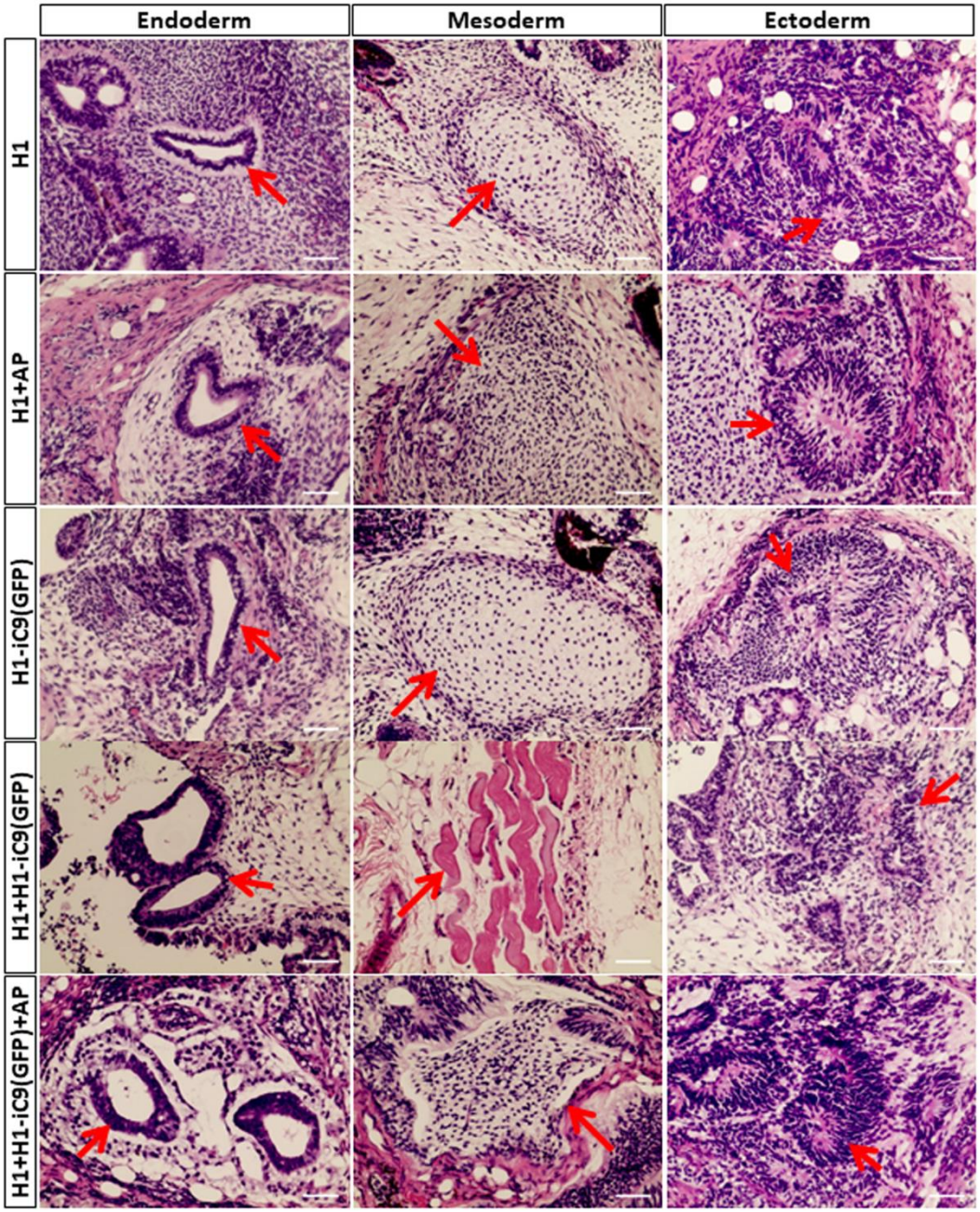

Figure S6. Teratoma formation in NSG mice with H1-iC9(GFP) cells, related to Figure 2.

Representative H&E staining of teratoma sections derived from indicated cells exhibits all three germ layers (arrows). Scale bar = 50 μm.

Figure S7

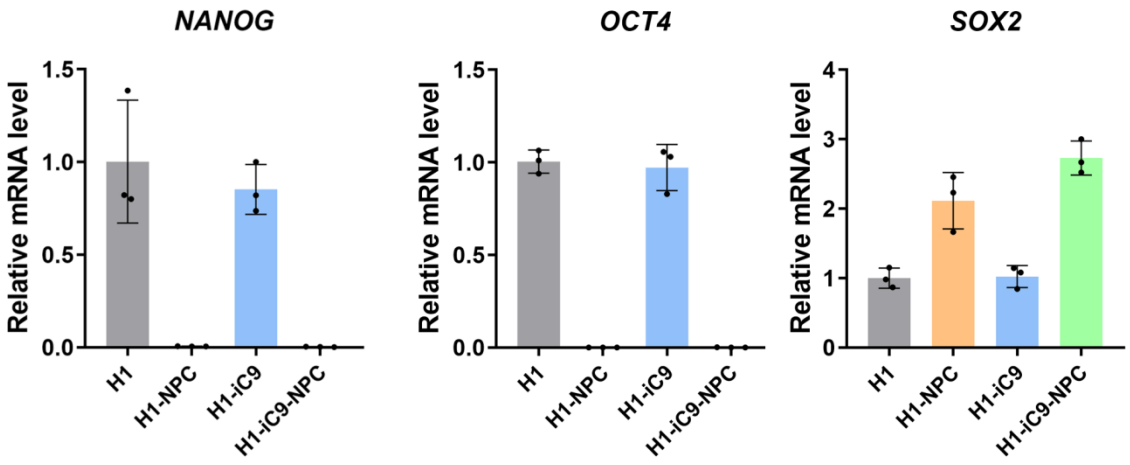

Figure S7. Relative expression of NANOG, OCT4 and SOX2 in undifferentiated cells and NPCs quantified by qRT-PCR, related to Figure 4. Graphs present the mRNA level normalized to the control group (H1) ± s.d. from three independent experiments.

Figure S8

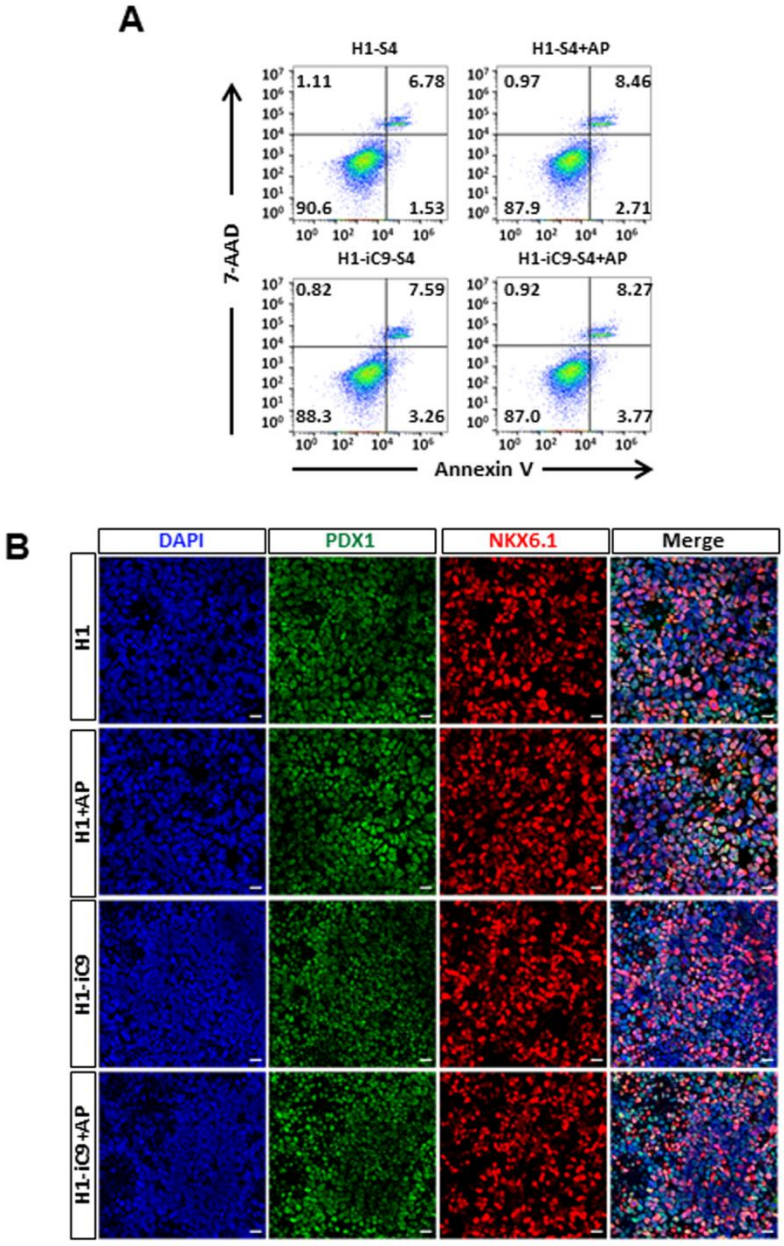

Figure S8. Viability of stage 4 pancreatic progenitor cells derived from H1 and H1-iC9 is not affected by AP1903 treatment, related to Figure 5. (A) Analysis of apoptotic cells in stage 4 pancreatic progenitor population derived from either H1 or H1-iC9 cells after overnight treatment with 10 nM AP1903. Result shown is representative of two independent experiments. (B) Representative immunofluorescence staining of $PDX1^{+}$ and $NKX6.1^{+}$ pancreatic progenitor

cells in the stage 4 population either mock treated or treated with 10 nM AP1903 overnight. Scale bar = 20 μm.

Figure S9

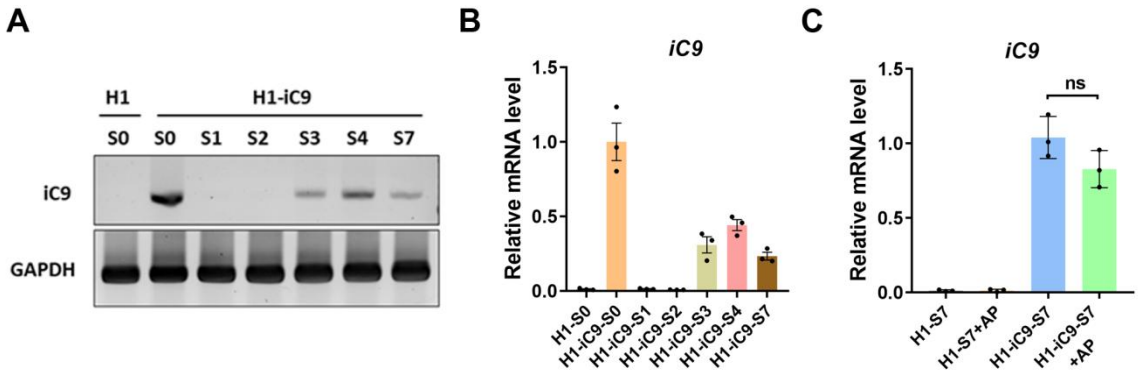

Figure S9. Transcription of transgene iC9 during beta-like cell differentiation, related to Figure 6. (A) Semi-quantitative RT-PCR analysis of the SOX2-iC9 fusion transcript in cells at the indicated differentiation stage. (B) Relative expression of the iC9 transgene in the indicated cells. The graph presents mean mRNA levels ± s.d. from three independent experiments normalized to the level in H1-iC9-S0 cells. (C) Relative expression of iC9 transgene in the S7 cells derived from H1 or H1-iC9 cells with and without AP1903 treatment, as measured by qRT-PCR (N=3). Data represents the mean ± s.d. ns: not statistically significant.

Figure S10

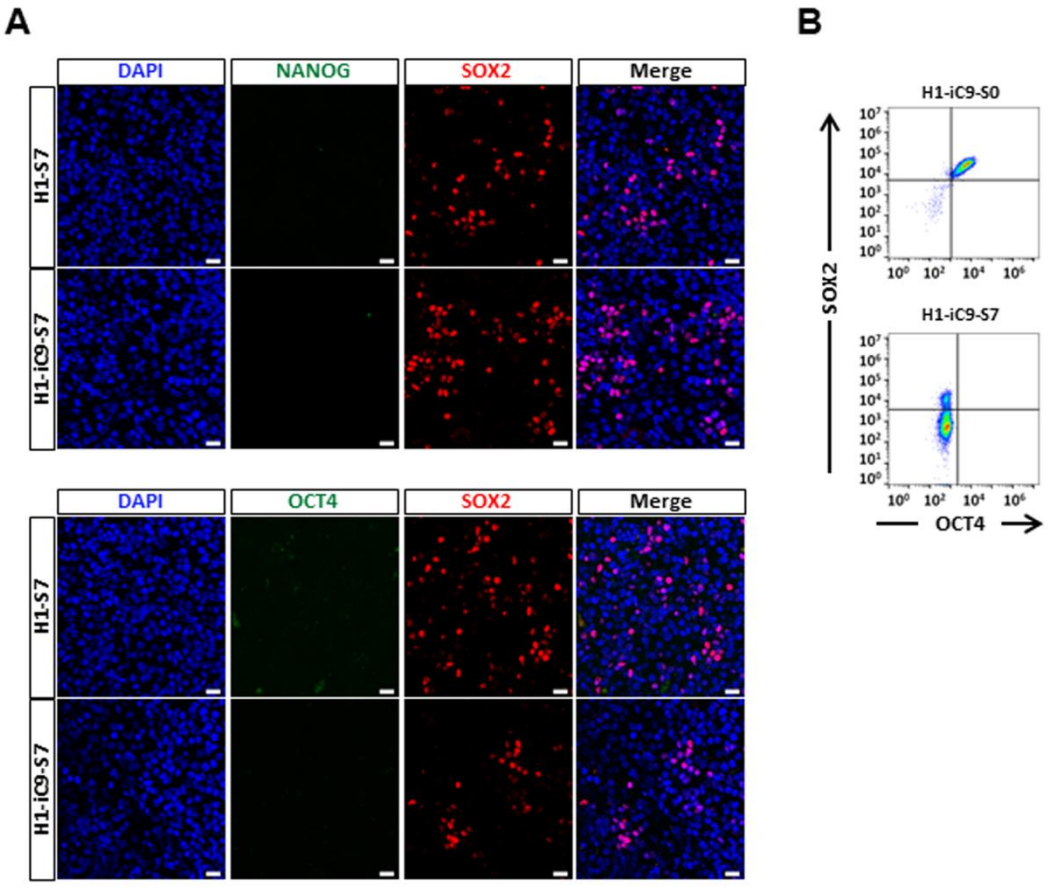

Figure S10. SOX2$^+$ cells in the S7 population are not undifferentiated stem cells, related to Figure 6. (A) Stage 7 cell populations derived from H1 and H1-iC9 differentiation were co-stained with antibodies against NANOG, OCT4, and SOX2 and detected by fluorescence microscopy. Scale bar = 20 μm. (B) Flow cytometry analysis of SOX2$^+$/OCT4$^+$ cells in the S0 and S7 populations derived from H1-iC9 cells. Result shown is a representative of two independent experiments.

Figure S11

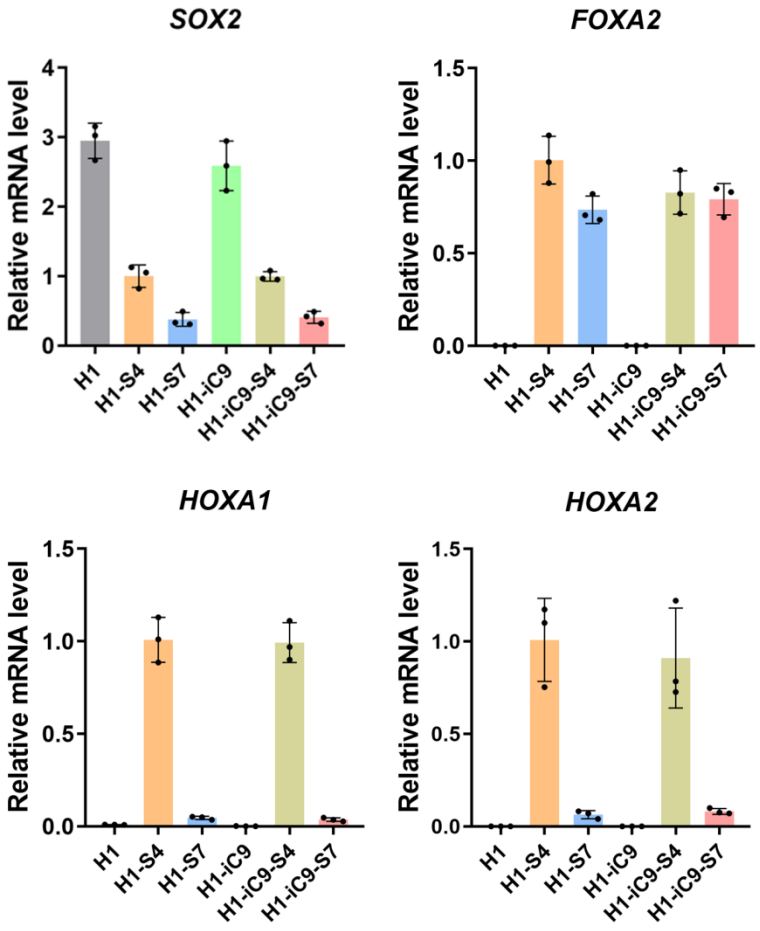

Figure S11. Relative mRNA level of SOX2, FOXA2, HOXA1 and HOXA2 in the indicated cells, related to Figure 6. Data are presented as the fold change relative to H1-S4 cells (N=3 biological replicates).

SUPPLEMENTAL TABLES

Table S1. Sequencing analysis of predicted off-target sites, related to Figure 1.

Genomic location	CRISPR Target Sequence	Sequencing results
chr3:181713280 (on target)	CCATTAACGGCACACTGCCCCTC	
chr8:124301775	CCATTAACGaCACACTGCCCCTC	WT
chr12:116042336	GAGGGGCAGgaTGCCtTTAATGG	WT
chr14:74269072	GAGGGGCAGaGTaCCGTgAAAGG	WT
chr19:44685040	GAGGGGCAGgGTGCtGTgAAAGG	WT
chr2:127627389	GAGGGGCAGTGTGCCGTcccGGG	WT
chr3:181713318 (on target)	CCGGACAGCGAACTGGAGGGGGG	
chr3:136862390	CCCCCCTtCAGTcCGCTGTCCGt	WT
chr10:49752274	CCGGgCAGCaAAgTGGAGGGAGG	WT
chr17:30210703	CaGGACAGtGAACaGGAGGGAGG	WT
chr5:443399	CCGGACcGgGAcCTGGAGGGCGG	WT
chr6:31781643	CCACCCTCCAGTcCcCTGTCCcG	WT

Table S2. Primers used in this study, related to Figure 1-3 and Figure 6.

Primers for plasmid construction

Donor plasmid	PCR Fragments	Primer set
2A-iC9-Puro	Left arm	FP: CCATCGATGAACCAGCGCATGGACAGTTAC RP: GCTCTAGACATGTGTGAGAGGGGCAGTGTGCCGTTAATAGCCGTGCCGG
	Right arm	FP: GCTCTAGAAAGCTTGGATCCAGAAATTTTCAAAGAAAAACGAGGGAAAT RP: AAGGAAAAAAGCGGCCGCGCAAGAAGCCTCTCCTTGAAAAATATT
	2A	FP: AAGGAAAAAAGCGGCCGCTCTAGACTCGAGGGCAGCGGCGCCACGAACTTC RP: AGATAGTCTCCACCTGCACTCCAGGACCGGGGTTTTCTT
	FKBP	FP: ATAAGAATGCGGCCGCAATGGGAGTGCAGGTGGAGACTATCT RP: GTCGACTCCGGATCCACCGCCAGATTCCAGTTTTAGAA

	2A-FKBP	FP: AAGGAAAAAAGCGGCCGCTCTAGACTCGAGGGCAGCGGCGCCACGAACTTC RP: GTCGACTCCGGATCCACCGCCAGATTCCAGTTTTAGAA

Primers for Surveyor assay

Target Gene	Primer set	Expected PCR product (bp)	Expected cleaved products (bp)
SOX2	FP: TGCAGGACCAGCTGGGCTAC RP: CGTGAGTGTGGATGGGATTGGT	581	405, 176

Primers for clone screening

Target Gene	PCR region	Primer set
SOX2	Left arm junction	LA-FP1: GCGGCAATAGCATGGCGA LA-RP1: AGATAGTCTCCACCTGCACTCCCATAGGACCGGGGTTTTCTT
	Right arm junction	RA-FP1: GTGTCTCTCACTCGGAAGGACAT RA-RP1: TCTTCTTTTCACGTTTGCAACTGTC
	Monoallelic and biallelic gene insertion	LA-FP2: CCATGGGTTCGGTGGTCAAGT RA-RP2: CGTGAGTGTGGATGGGATTGGT
	Puromycin-resistant gene deletion	Cre-FP1: TCCTGGTACGTTGAGACCCTGG Cre-RP1: CGTGAGTGTGGATGGGATTGGT

Primers for RT-PCR

Target Gene	Primer set	Expected PCR product size (bp)
SOX2	FP: GGGAAATGGGAGGGGTGCAAAAGAGG RP: TTGCGTGAGTGTGGATGGGATTGGTG	151
SOX2 fusion transcript	FP: CCATGGGTTCGGTGGTCAAGT RP: CCACATCGAAGACGAGAGTGG	621
OCT4	FP: TCGAGAACCGAGTGAGAGG RP: GAACCACACTCGGACCACA	125
NANOG	FP: ATGCCTCACACGGAGACTGT RP: AAGTGGGTTGTTTGCCTTTG	103
iC9	FP: CAGGAGACGTGGAAGAAAACCCC RP: TAGTGCACCACGCAGGTCTGG	109
FOXA2	FP: GGAGCAGCTACTATGCAGAGC RP: CGTGTTCATGCCGTTCATCC	83
PAX9	FP: GGAGGAGTGTTCGTGAACGG RP: CGGCTGATGTCACACGGTC	98
HOXA1	FP: TCCTGGAATACCCCATACTTAGC RP: GCACGACTGGAAAGTTGTAATCC	95

HOXA2	FP: ACCCCGAAGGGTGGAGATT RP: CGGAGTCCTCAAGGCTTTTACAT	152
GAPDH	FP: TGCACCACCAACTGCTTAGC RP: GGCATGGACTGTGGTCATGAG	87

Table S3. Antibodies for flow cytometry and immunofluorescence staining, related to Figure 2-6.

Antibodies for flow cytometry

Conjugated antibody	Source	Dilution
FITC Mouse anti-CD45	BioLegend	1:40
Alexa Fluor 647 Mouse anti-SOX2	BD Biosciences	1:40
PE Mouse anti-Oct3/4	BD Biosciences	1:10
Alexa Fluor 647 Mouse anti-NKX6.1	BD Biosciences	1:40
PE Rabbit anti-Insulin	Cell Signaling Technology	1:100
Alexa Fluor 647 Mouse IgG1, κ isotype control	BD Biosciences	1:40
PE Mouse IgG1, κ Isotype Control	BD Biosciences	1:10
PE Rabbit IgG1 XP isotype control	Cell Signaling Technology	1:100

Antibodies for immunofluorescence staining

Primary antibodies			
Antigen	Species	Source	Dilution
Nestin	Rabbit	EMD Millipore	1:500
NANOG	Mouse	BD Biosciences	1:500
OCT4	Rabbit	Stemgent	1:500
SOX2	Rabbit	Novus Biology	1:250
SOX2	Goat	R&D System	1:100
TUJ1	Rabbit	Covance	1:1000
PDX1	Rabbit	Abcam	1:500
NKX6.1	Mouse	BCBC #2023	1:500
MAFA	Rabbit	Abcam	1:500
Insulin	Guinea Pig	Dakocytomation	1:1000
GFP	Chicken	Abcam	1:2000
HA	Rabbit	Cell Signaling Technology	1:800
FOXA2	Goat	R&D System	1:25
Secondary antibodies			
Antigen	Conjugation	Source	Dilution
Rabbit/Mouse/Chicken	Alexa Fluor 488	Jackson ImmunoResearch	1:1000

Goat/Rabbit	Cy3	Jackson ImmunoResearch	1:2000
Guinea Pig/Sheep	Cy5	Jackson ImmunoResearch	1:500

Table S4. Protocol for H1 differentiation into stage 7 beta-like cells, related to Figure 5.

Stage	Day	Basic medium	Factors
Stage 1	Day 1	MCDB 131 1x Glutamax 10 mM Glucose 1.5 g/L Sodium bicarbonate 0.5% BSA	100 ng/mL GDF8 (PeproTech) 3 µM CHIR99021 (SellechChem)
	Day 2	MCDB 131 1x Glutamax 10 mM Glucose 1.5 g/L Sodium bicarbonate 0.5% BSA	100 ng/mL GDF8 0.3 µM CHIR99021
	Day3	MCDB 131 1x Glutamax 10 mM Glucose 1.5 g/L Sodium bicarbonate 0.5% BSA	100 ng/mL GDF8
Stage 2	Day4-5	MCDB 131 1x Glutamax 10 mM Glucose 1.5 g/L Sodium bicarbonate 0.5% BSA	50 ng/mL FGF7 (PeproTech) 0.25 mM ascorbic acid (Sigma)
Stage 3	Day 6-7	MCDB 131 1x Glutamax 10 mM Glucose 2.5 g/L Sodium bicarbonate 2% BSA	50 ng/mL FGF7 0.25 mM ascorbic acid 0.25 µM SANT-1 (Sigma) 1 µM retinoic acid (Sigma) 100 nM LDN193189 (Stemgent) 1:200 ITS-X (Life technologies) 200 nM TPB (Millipore)
Stage 4	Day 8-10	MCDB 131 1x Glutamax 10 mM Glucose 2.5 g/L Sodium bicarbonate 2% BSA	2 ng/mL FGF7 0.25 mM ascorbic acid 0.25 µM SANT-1 0.1 µM retinoic acid 200 nM LDN193189 1:200 ITS-X 100 nM TPB
Stage 5	Day 11-13	MCDB 131 1x Glutamax 20 mM Glucose 1.5 g/L Sodium bicarbonate 2% BSA	0.25 µM SANT-1 0.05 µM retinoic acid 100 nM LDN193189 1:200 ITS-X 1 µM T3 (Sigma) 10 µM ALK5i (Enzo Life Sciences) 10 µM zinc sulfate (Sigma) 10 µg/mL heparin (Sigma)
Stage 6	Day 14-20	MCDB 131 1x Glutamax 20 mM Glucose 1.5 g/L Sodium bicarbonate	100 nM LDN193189 1:200 ITS-X 1 µM T3 10 µM ALK5i

		2% BSA	10 µM zinc sulfate 100 nM Gs inh XX (EMD Millipore) 10 µg/mL heparin
Stage 7	Day 21-27	MCDB 131 1x Glutamax 20 mM Glucose 1.5 g/L Sodium bicarbonate 2% BSA	1:200 ITS-X 1 µM T3 10 µM ALK5i 10 µM zinc sulfate 1 mM N-acetyl cysteine (Sigma) 10 µM Trolox (EMD Millipore) 2 µM R428 (SelleckChem) 10 µg/mL heparin

TRANSPARENT METHODS

Plasmid construction

Cas9(phCas9) (Mali et al., 2013) and Cas9 D10A (phCas9-D10A) (Mali et al., 2013) expression plasmids were purchased from Addgene (Cambridge, MA). The CRISPR plasmid, pU6-CRISPR, containing the U6 promoter and the gene for the single-guide RNA (sgRNA) was generated as previous described (Wang et al., 2015). To generate the donor plasmid for in-frame insertion of the *iC9* gene into the *SOX2* locus, left and right homology arms sequences (~0.5 kb of each) spanning the stop codon of the *SOX2* gene were PCR amplified from the genomic DNA of H1 cells and cloned into pBluescript SK(-) to generate pBS-SOX2-HA. The 1.3 kb *2A-iC9* gene was constructed by in-frame fusion of the PCR amplified *iC9* gene in pMSCV-F-del Casp9. IRES.GFP (Addgene) (Straathof et al., 2005) with a 57-bp synthetic fragment encoding the 2A peptide. The *2A-iC9* cassette was then cloned into pBluescript SK(-) to generate pBS-2A-iC9. To construct the donor plasmid, pBS-SOX2-HA was linearized by Xba1 and BamH1 double digestion. A 1.3 kb fragment containing the *2A-iC9* gene was isolated from pBS-2A-iC9 by Xba1 and Kpn1 double digestion. A 1.6 kb fragment containing the pgk-Puro fragment flanked by loxP recognition sites was isolated from ppgk-Puro by Kpn1 and BamH1 digestion. The three fragments were ligated to generate pSOX2-iC9-donor. All primers used for plasmid construction are listed in Table S2.

DNA transfection

HEK293T cells were cultured in DMEM (Lonza, Allendale, NJ) supplemented with 10% fetal bovine serum (HyClone, Logan, UT), 100 U/mL penicillin, and 100 mg/mL streptomycin. Cells were passaged twice a week at 37°C under 5% CO_2. For the Surveyor assay, HEK293T cells cultured in 48-well plates were transfected at 40% confluency using Lipofectamine 3000 (Life Technologies) together with 67 ng pU6-CRISPR and 200 ng of Cas9 or Cas9 D10A expression plasmid. Forty-eight hours after transfection, genomic DNA was isolated with Epicentre QuickExtract solution (Epicentre Biotechnologies, Madison, WI) and used for the Surveyor assay. Human ES cell line H1 (WA01) was purchased from WiCell Research Institute (Madison, WI). The cells were cultured in mTeSR1 medium (StemCell Technologies, Vancouver, BC) on plates coated with Matrigel (BD Bioscience, San Jose, CA). Cells were passaged with ReLeSR (STEMCELL Technologies) every 4-6 days with 1:6~1:12 dilutions. For DNA transfection, H1 cells pretreated overnight with Rho kinase (ROCK)-inhibitor Y-27632 (Stemgent, Beltsville, MD) were dissociated into single cells using Accutase (STEMCELL Technologies). Nucleofection was carried out using 4D Amaxa P3 Primary Cell 4-D Nucleofector system (Lonza). Approximately $8X10^5$ cells were nucleofected using program CA-137. To insert the *iC9* gene into the *SOX2* locus in H1 cells, 1.5 µg pSOX2-iC9-donor was nucleofected with 0.65 µg pU6-sgRNA1, 0.65 µg pU6-sgRNA2, and 2 µg pCas9 D10A. Two days after nucleofection, single cells were prepared and plated in mTeSR1 medium containing 0.5 µg/mL puromycin. Puromycin-resistant colonies were picked after two weeks of selection and genotyped with genomic PCR using primers listed in Table S2. To delete the pgk-Puro cassette, 4 µg pBS185 (Sauer, 1993) and 1 µg pmax-GFP^{TM} (Lonza) were introduced into cells by nucleofection. FACS sorted GFP^+ cells were plated and individual colonies picked after two weeks. Genomic PCR was performed to verify the deletion of the puromycin cassette. PCR primers used for genotyping the clones are listed in Table S2.

Surveyor assay

To carry out the Surveyor assay, the genomic DNA spanning the CRISPR cleavage site was PCR amplified with Hotstar Taq (Qiagen, Germantown, MD), and the PCR product was subjected to denaturation and reannealing with the following conditions: 95°C for 10 min, 95°C to 85°C ramping at –2°C/s, 85°C to 25°C ramping at – 0.25°C/s, and 25°C for 1 min. PCR primers for DNA amplification are listed in Table S2. Three microliter of re-annealed DNA in a 12 µL reaction was mixed with 1 µL of Surveyor Nuclease S (Integrated DNA Technologies, Skokie, IL), 1 µL of Surveyor Enhancer S, and 1.2 µL of 0.15 M $MgCl_2$ and incubated at 42°C for 1 h. The digested product was analyzed on a 2% agarose gel and imaged with a ChemiDoc imaging System (Bio-Rad Laboratories, Hercules, CA). The percentage of indel formation was calculated by the following formula: % indel formation = 100 × [1 − (1 − fraction cleaved)$^{1/2}$]; fraction cleaved = 100 × sum of the cleavage product peak / cleavage product + parent peak.

Lentiviral production and transduction

To generate the lentiviral vector HIV7/PGK-GFP, approximately 2 x 10^6 HEK293T cells were cotransfected with 12 µg pHIV7/PGK-GFP, 12 µg pCgp, 4 µg pRev-2, and 2 µg pCMV-G (Lo et al., 2007) using calcium phosphate coprecipitation. Infectious virus was harvested 48 h later and tittered on HT1080 cells with different dilutions in the presence of 4 µg/mL polybrene. FACS analysis was carried out 48 h after transduction to determine the fraction of GFP^+ cells.

Cytogenetic Analysis

ES cells at ~80% confluence in mTesR culture medium were processed for preparation of metaphase chromosome spreads according to standard cytogenetic protocols (Barch and Association of Cytogenetic Technologists., 1991). Following DAPI staining, metaphase chromosome spreads were observed and counted under a fluorescence microscope. Twenty metaphases were analyzed for each cell line.

Cell viability assay

H1, H1-iC9-pur and H1-iC9 cells were seeded in 96-well plate at a density of 10^4 cells /well in the absence or in the presence of varying concentrations of AP1903 overnight. Cell viability was determined by MTS assay using a CellTiter 96® AQueous One Solution kit (Promega, Madison, MI) according to the manufacturer's instructions.

Apoptosis assay

Apoptosis assay was performed after overnight incubation of cells with 10 nM AP1903. To block Caspase activity, the pan Caspase inhibitor qVD-OPh (20 µmol/l, ApexBio Technology, Boston, MA) was added together with AP1903. The percentage of apoptotic cells after overnight incubation was measured by staining the cells with Annexin V-PE and 7-amino actinomycin D (7-AAD) following the manufacturer's instruction (BD Pharmingen, San Jose, CA) and analyzed by flow cytometry. Annexin V^+/7-AAD^- and Annexin V^+/7-AAD^+ cells represent early and late apoptotic cells, respectively.

Teratoma formation

The stable H1-iC9(GFP) line was established by the transduction of H1-iC9 cells with HIV7/C-GFP at a multiplicity of infection of 2. GFP^+ cells were isolated and pooled by cell sorting 48 h after transduction. To induce teratoma, cells were dissociated with Accutase and resuspended in mTeSR1 medium containing 10 µM Y-27632. Approximately $2X10^6$ cells in 50 µL medium were mixed with 50 µL cold Matrigel (BD Pharmingen) and injected subcutaneously into the lateral flank of 8-12 week old NOD scid gamma (NSG) mice. Teratomas were harvested 4-6 weeks after cell injection, fixed in 10% neutralized formalin for 24 h, embedded in paraffin, and

sectioned for hematoxylin-eosin (H&E) staining. Animal studies were carried out in accordance with protocols approved by the City of Hope Institutional Animal Care and Use Committee.

Semi-quantitative RT-PCR and real-time RT-PCR

Total RNA was isolated using the RNeasy mini kit (Qiagen) following the manufacturer's instructions. The purity and concentration of RNA were determined using a Nanodrop spectrophotometer (NanoDrop Technologies, Wilmington, DE). Total RNA (1 µg) was reverse transcribed into cDNA using SuperScript VILO MasterMix (Life Technologies). For semi-quantitative PCR, 5 µL diluted cDNA (1:25) was amplified using HotStar Taq polymerase. The products were separated on a 2% agarose gel and imaged with ChemiDoc imaging System. Real-time RT-PCR was carried out in the CFX96 Touch^{TM} Real-time PCR Detection System (Bio-Rad) using SYBR Green Supermix (Bio-Rad). Primers used for RT-PCR are listed in Table S2.

Flow cytometry analysis

To detect CD45^{+} hematopoietic cells, both H1- and H1-iC9-derived hematopoietic cell populations were suspended in flow cytometry staining buffer (Thermo Fisher Scientific, Irwindale, CA). FITC-conjugated anti-human CD45 antibody (Biolegend, San Diego, CA) at a 1:40 dilution was added and the mixture incubated for 30 min at room temperature. For the staining of intracellular antigens, cells in suspension were fixed and permeabilized using Foxp3 transcription factor staining kit (Thermo Fisher Scientific). After washing with permeabilization buffer, cells were stained with directly conjugated antibodies. Antibodies and dilutions used for FACS are listed in Table S3. The data for FACS was collected using an Accuri C6 flow Cytometer (BD Biosciences) and analyzed with the FlowJo software.

Immunofluorescence staining

For cell immunofluorescence staining, monolayer cultures were fixed in 4% paraformaldehyde for 15 min at room temperature and washed with PBS three times, followed by incubation for 1 h in blocking solution containing 5% BSA and 0.3% Triton X-100 in PBS. Primary and secondary antibodies were diluted with 1% BSA and 0.15% Triton X-100 in PBS. Cells were incubated with primary antibodies at 4°C overnight. After three washes with PBS, cells were incubated with fluorescence-conjugated secondary antibodies for 1 h at room temperature. After three washes with PBS, the cell-containing slide was mounted with mounting reagent and stained with DAPI (Vector Laboratories, Burlingame, CA). Images were captured using a Zeiss Axio Imager microscope (Carl Zeiss, San Diego, CA)**.** For the staining of H1- and H1-iC9-derived beta-like cells, cell clusters in S7 were removed from air-liquid interface, washed with PBS, and fixed in 4% paraformaldehyde solution at 4°C for 1 h. After three washed with PBS, cell clusters were incubated in 30% sucrose at 4°C overnight, embedded in OCT compound (Sakura, Torrance, CA), and frozen in dry ice. Sections (5 μm thickness) were prepared using a cryostat (Leica, Allendale, NJ). Slides were washed with PBS to remove OCT compound followed by incubation with blocking solution and stained with primary and secondary antibodies as described above. For paraffin-embedded teratoma staining, sections were deparaffinized in Clearify™ (American MasterTech, Lodi, CA), rehydrated with a gradient of ethanol, and underwent antigen retrieval in citrate buffer (PH 6.0) before blocking and antibody staining. Primary and secondary antibodies are listed in Table S3.

Western blot

Harvested cells were lysed using RIPA buffer (Thermo Fisher Scientific) containing HALT™ Protease Inhibitor Cocktail (Thermo Fisher Scientific). The cell lysates were mixed with 4xNuPAGE LDS sample buffer (Invitrogen, Carlsbad, CA) and loaded onto a NuPAGE 4–12%

Bis-Tris gel (Invitrogen) for protein separation. Proteins were transferred to polyvinylidene fluoride (PVDF) membranes (Bio-Rad) and blocked for 1 h with 5% BSA and 0.05% Tween in PBS followed by the incubation with a BCL-2 (50E3) rabbit antibody (1:1000, Cell Signaling Technology, Danvers, MA) or a mouse GAPDH antibody (1:2000, GeneTex, Irvine, CA) diluted with blocking solution at 4^0C overnight. Membranes were washed with PBS and incubated with HRP-conjugated secondary antibodies (Thermo Fisher Scientific) at room temperature for 1 h and developed using Pierce ECL substrate (Thermo Fisher Scientific).

Hematopoietic cell differentiation

Undifferentiated human H1 cells or H1-iC9 cells were induced to differentiate into $CD45^+$ cells as previously described (Senju et al., 2011). Briefly, undifferentiated cells were transferred onto OP9 feeder layers and cultured with α-Minimal Essential Medium (Hyclone) supplemented with 20% fetal calf serum. After 18 days, cells were detached with dissociation solution containing 0.25% trypsin, 0.1% collagenase type IV (Sigma), and 0.1% DNase I (Sigma) in PBS. Cells were passed through 100 µm cell strainers (Corning, Corning, NY) to yield a single-cell suspension, followed by culturing the cell suspension in α- Minimal Essential Medium containing 100 ng/mL GM-CSF and 50 ng/mL M-CSF (PeproTech, Rocky Hill, NJ) for 14 days.

Neuronal cell differentiation

Approximately 3 x 10^6 Accutase-dissociated single cells were suspended in 1ml neural induction medium consisting of STEMdiff™ Neural Induction Medium and SMADi Neural Induction Supplement (STEMCELL Technologies). Embryoid bodies (EBs) were harvested with 37 µm Reversible Strainers 5 days later followed by seeding into plates coated with Poly-L-ornithine (PLO) and laminin (Sigma) in STEMdiff™ Dopaminergic Neuron Differentiation Medium (STEMCELL Technologies). Neuronal rosettes that emerged were selectively removed with STEMdiff™ Neural Rosette Selector Reagent (STEMCELL Technologies) after 6 days in

culture. Rosettes were then replated into a new PLO/laminin-coated well and expanded for additional 7 days in STEMdiff™ Dopaminergic Neuron Differentiation Medium to generate neuronal precursors. Neuron precursors were frozen in culture medium supplemented with 10% DMSO. To generate neurons, frozen neuronal precursors were thawed and expanded for additional 7 days. The cells were then dissociated with Accutase and plated into PLO/laminin-coated 24-well plates at a density of 4~6 x 10^5/cm^2 in STEMdiff™ Dopaminergic Neuron Maturation Medium 1 (STEMCELL Technologies) for 2 days. AP1903 was added on the third day after the initiation of the maturation process. SOX2 expression was then examined 2 days after AP1903 treatment.

Beta-like cell differentiation

Human beta-like cells were differentiated from H1 and H1-iC9 cells using a seven-stage differentiation protocol reported by Rezania *et al*. (Rezania et al., 2014). Before differentiation, approximately 1.3-1.5 x 10^5 cells/cm^2 undifferentiated cells were seeded into Matrigel-coated plates in mTeSR medium supplemented with 10µM Y27632. After 48 h, cell differentiation was initiated by replacing the culture media with MCDB 131 media (Corning) supplemented with Glutamax (Life Technologies), fatty acid-free BSA (Proliant Biologicals, Boone, IA), and a cocktail of molecules described in Table S4 with fresh media change every day. Cells were cultured in monolayer during the first four stages of differentiation to generate pancreatic progenitor cells in stage 4. The stage 4 cells were dissociated with TrypLE Express Enzyme (Life Technologies) and resuspended in stage 5 media at a density of 5 x 10^7/mL. Approximately 10 µL cell drops containing 5 x 10^5 cells were spotted onto a filter insert (Corning) floating in 1.5 ml stage 5 differentiation media. Cells cultured in this air-liquid interface were allowed to differentiate into stage 7 with media change every day. Cell clusters were removed from the insert for analysis between 28~35 days after the initiation of differentiation.

Statistical analysis

Results are presented as mean ± standared deviation (s.d.). Statistical significance between groups was calculated using one-way ANOVA followed with Turkey's correction. *P<0.05, **P<0.01, ***P<0.001, ****P<0.0001, ns: P value not significant. Statistic calculations were conducted using GraphPad Prism 7 software (GraphPad Software, San Diego, CA). The number of independent experiments was indicated in figure legends.

SUPPLEMENTAL REFERENCES

Barch, M.J., and Association of Cytogenetic Technologists. (1991). The ACT cytogenetics laboratory manual, 2nd edn (New York: Raven Press).

Lo, H.L., Chang, T., Yam, P., Marcovecchio, P.M., Li, S., Zaia, J.A., and Yee, J.K. (2007). Inhibition of HIV-1 replication with designed miRNAs expressed from RNA polymerase II promoters. Gene Ther *14*, 1503-1512.

Mali, P., Yang, L., Esvelt, K.M., Aach, J., Guell, M., DiCarlo, J.E., Norville, J.E., and Church, G.M. (2013). RNA-guided human genome engineering via Cas9. Science *339*, 823-826.

Rezania, A., Bruin, J.E., Arora, P., Rubin, A., Batushansky, I., Asadi, A., O'Dwyer, S., Quiskamp, N., Mojibian, M., Albrecht, T.*, et al.* (2014). Reversal of diabetes with insulin-producing cells derived in vitro from human pluripotent stem cells. Nature biotechnology *32*, 1121-1133.

Sauer, B. (1993). Manipulation of transgenes by site-specific recombination: use of Cre recombinase. Methods Enzymol *225*, 890-900.

Senju, S., Haruta, M., Matsumura, K., Matsunaga, Y., Fukushima, S., Ikeda, T., Takamatsu, K., Irie, A., and Nishimura, Y. (2011). Generation of dendritic cells and macrophages from human induced pluripotent stem cells aiming at cell therapy. Gene Ther *18*, 874-883.

Straathof, K.C., Pule, M.A., Yotnda, P., Dotti, G., Vanin, E.F., Brenner, M.K., Heslop, H.E., Spencer, D.M., and Rooney, C.M. (2005). An inducible caspase 9 safety switch for T-cell therapy. Blood *105*, 4247-4254.

Wang, X., Wang, Y., Wu, X., Wang, J., Wang, Y., Qiu, Z., Chang, T., Huang, H., Lin, R.J., and Yee, J.K. (2015). Unbiased detection of off-target cleavage by CRISPR-Cas9 and TALENs using integrase-defective lentiviral vectors. Nature biotechnology *33*, 175-178.